



Trends and amount changes of temperature and precipitation under future projections in high–low groups and intra-period for the Eastern Black Sea, the Wettest Basin in Türkiye

Sinan Nacar¹ · Murat Şan² · Murat Kankal³ · Umut Okkan⁴

Received: 4 December 2023 / Accepted: 25 March 2024
© The Author(s) 2024

Abstract

This study investigates the possible effects of climate change on temperature and precipitation variables in the Eastern Black Sea Basin, Türkiye’s wettest and flood-prone region. The outputs of three GCMs under historical, RCP4.5, and RCP8.5 scenarios were down-scaled to regional scale using the multivariate adaptive regression splines method. The future monthly temperature and precipitation for 12 stations in the basin were projected for three periods: the 2030s (2021–2050), 2060s (2051–2080), and 2090s (2081–2100). In addition to relative changes, high and low groups and intra-period trends were analyzed for the first time using innovative methods. For the pessimistic scenario, an increase of 3.5 °C in the interior and 3.0 °C in the coastal areas of the basin is projected. For the optimistic scenario, these values are expected to be 2.5 and 2.0 °C, respectively. A decrease in precipitation is projected for the interior region, and a significant increase is expected for the eastern and coastal areas of the basin, especially in spring. This result indicates that floods will occur frequently coastal areas of the basin in the coming periods. Also, although the monotonic trends of temperatures during periods are higher than precipitation in interior regions, these regions may have more uncertainty as their trends are in different directions of low and high groups of different scenarios and GCMs and contribute to all trends, especially precipitation.

Keywords Eastern Black Sea Basin · Climate change · Innovative trend analysis · Multivariate adaptive regression splines · Statistical downscaling

1 Introduction

In recent years, depending on the development of technology and the increase in population, industrialization, consumption, and environmental destruction have increased rapidly. Such increases have also raised greenhouse gas emissions, the most significant cause of the change in the world climate (Nourani et al. 2019). The effects of changes in the climate of the regions on the hydrological cycle and, therefore, on water resources have critical importance because all life and ecosystems depend on water (Günen and Atasever

Extended author information available on the last page of the article

2024; Mekonnen and Disse 2018; Semadeni-Davies et al. 2008). For this reason, planners need to determine how existing water resources will be affected under changing climatic conditions, use resources under changing conditions, and prepare new water resource strategies for future periods. This is achieved by obtaining information about the impact of climate change on hydro-meteorological variables at a local scale (Al-Mukhtar and Qasim 2019). Investigating how precipitation and temperature values, the most influential variables of the hydrological cycle and climate, will change under the effects of climate change in the future can help decision-makers make effective decisions to overcome problems such as drought and floods (Nourani et al. 2019).

General circulation models (GCMs) are the most reliable tools to predict future climate based on socio-economic and demographic factors corresponding to different emission scenarios (Araya-Osses et al. 2020; Ouhamdouch and Bahir 2017). However, one of the main problems encountered in evaluating the effects of climate change with the outputs of GCMs is that the resolutions of these models are coarse (250 to 600 km). In addition, GCMs cannot capture the regional processes in the regions, where mountain ranges are located and cannot appropriately include the orographic features of these regions in the calculations (Campozano et al. 2016). These data cannot be used directly to analyze the effects of hydrological and environmental climate change factors on a regional scale (Okkan and Inan 2015b; Ouhamdouch and Bahir 2017; Wilby et al. 2002). Therefore, these coarse-resolution GCMs must be downscaled to higher spatial and temporal resolution (Al-Mukhtar and Qasim 2019). Downscaling methods have emerged to downscale large-scale atmospheric variables to local-scale meteorological variables (Huang et al. 2011). Downscaling methods are divided into two groups in the literature: dynamic and statistical downscaling methods (Okkan and Kirdemir 2016; Wilby et al. 1998). Dynamic downscaling is based on physical climate models operated on a regional scale. These models take the initial and boundary conditions from the GCM outputs and can be run at higher resolutions, considering their topographic features (Crane and Hewitson 1998; Okkan and Inan 2015a). However, the computational costs of dynamic downscaling methods are quite high compared to statistical methods. In addition, this method includes certain parameterization processes to obtain higher-resolution data from the given data set (Araya-Osses et al. 2020; Huang et al. 2011). Statistical downscaling methods establish statistical or empirical relationships between atmospheric variables in GCMs and meteorological variables measured at station scale. These methods are inexpensive, easily applicable to different regions, have low computational costs, and are frequently used in climate change impact, risk, and uncertainty studies. The disadvantage of statistical downscaling methods is that they require a sufficient length of observed historical data (Huang et al. 2011; Wilby et al. 2002). Wilby and Wigley (1997) and Chen et al. (2011) have extensive details on the advantages and disadvantages of the two downscaling methods.

Wilby and Wigley (1997) divided statistical downscaling methods into three classes: regression, weather-type approaches, and stochastic weather generators, respectively. In recent years, various statistical downscaling methods, i.e., artificial neural networks, gene expression programming methods, least-squares support vector machines, stochastic weather generators, have been used in different parts of the world due to their ease of use (Fiebig-Wittmaack et al. 2012; Fistikoglu and Okkan 2011; Guven et al. 2021; Huang et al. 2011; Souvignet et al. 2010). However, the interpretability of the methods used is either non-existent or low. For these reasons, multivariate adaptive regression splines (MARS) offers the opportunity to explain the importance of variables and the relationships between

them (Huang et al. 2020; Şan et al. 2023; Zhang et al. 2021), based on the regression-type statistical downscaling method, was preferred in this study.

Beyond the analysis of future quantitative and proportional statistical values of hydro-meteorological variables, water resources management and planning also place significant emphasis on the investigation of trends that provide a chance for a detailed examination of climate change (Şan et al. 2021; Şen 2012). Monotonic trend methods are generally preferred in trend analysis for future scenarios (Nuri Balov and Altunkaynak 2020; Pechlivanidis et al. 2017; Yao et al. 2020). However, the study of trends of low and high values of hydrometeorological variables that provide information about events such as droughts and floods (Dabanli et al. 2016; Okkan et al. 2024) has been neglected.

This study aims to determine the effects of climate change on regional temperature and precipitation variables statistically and in terms of intra-period monotonic and group trends by using the statistical downscaling method for the first time. Within the scope of this study, monthly mean temperature and total precipitation data for the 2021–2100 period were produced and evaluated for 12 meteorology stations in the Eastern Black Sea Basin (EBSB) that received the highest precipitation in Türkiye. To this end, the MARS statistical downscaling method was used with monthly observation data from the meteorological stations using large-scale ERA-Interim predictors. Then, the calibrated downscaling model was applied to project the temperature and precipitation for three future periods using three GCMs (CNRM-CM5.1, HadGEM2-ES, and MPI-ESM-MR) outputs under RCP4.5 and RCP8.5 emission scenarios. Finally, intra-period monotonic trend analyses and the trends of low and high values that increase the probability of drought and flood (Dabanlı et al. 2016) were examined. The methodology presented in the study is thought to be useful in evaluating the effects of climate change on temperature and precipitation parameters in future periods at the basin scale. The outputs obtained from this study can be used in watershed modeling studies, water resources planning and management, reservoir operation, future trend analysis, and water budget planning for the basin.

2 Study area and data sets

2.1 Study area

Türkiye is situated in an area characterized by mild climatic conditions. However, because it is surrounded by seas on three sides, landforms, and especially the mountains extending parallel to the coasts, it experiences quite different climatic conditions. Türkiye is divided into 25 large hydrological basins (Fig. 1) (Bayer Altin and Altin 2021). The EBSB is situated on the northeast coast of Türkiye and receives a lot of precipitation due to its geographical features and location. Many floods and deaths have occurred after short-term heavy precipitation in the EBSB (Aliyazıcıoğlu et al. 2023; Haltas et al. 2021; Yüksek et al. 2013). Also, it has a very high energy potential within the country (Akçay et al. 2022). Due to these circumstances, it is among the most vulnerable regions to the effects of climate change. Therefore, it is one of Türkiye's most important hydrological basins.

The total area of the basin is 24,077 km², and it is geographically located between 40° 15' and 41° 34' north latitude and 36° 43' and 41° 35' east longitude (Fig. 2). The basin is surrounded by the Black Sea in the north, Kaçkar Mountains in the east, Yamanlı, Soğanlı, Kemer, and Iğdır Mountains in the south, and extends to the east of Çarşamba Plain in the

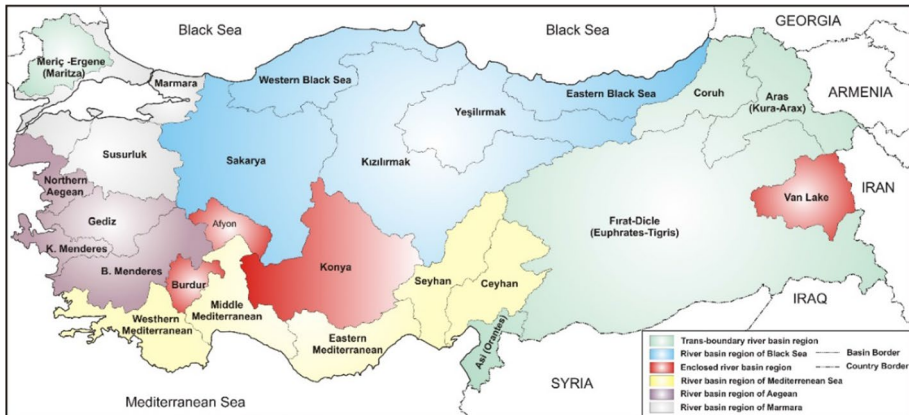


Fig. 1 Hydrological basins in Türkiye

west. With a mean annual surface water potential of $16.46 \times 10^9 \text{ m}^3$, the EBSB is of prime importance compared to a yearly mean groundwater potential of $0.49 \times 10^9 \text{ m}^3$ (Anılan et al. 2016; Bayazit and Avcı 1997; Nacar et al. 2020; Yüksek et al. 2013).

The highest precipitation falls around Rize, Pazar, and Hopa on the basin's northeast coastline. Although the basin's annual average total precipitation amount is 1100 mm, the value is 2300 mm at the stations in this region. There are many streams of various sizes within the borders of the EBSB. These streams flow into the Black Sea through steep slopes and deep valleys. As a result of the melting of the snow in the mountainous regions due to the increase in temperature and heavy precipitation falling on the slopes of the mountains, massive and destructive floods have occurred in the basin, which comprises six provinces: Giresun, Trabzon, Rize, Artvin, Gümüşhane, and Bayburt (Ghiaei et al. 2018). During the 90 years from 1930 to 2020, 2101 flood events occurred in Türkiye, and 206 people died. The first two districts where the most flood events occurred are the Pazar and Çayeli districts, located in the EBSB and within the borders of Rize province (Haltaş et al. 2021). According to the results of climate change impact studies, it is predicted that 450×10^6 people and $430 \times 10^3 \text{ km}^2$ of agricultural land will be affected by floods by 2050 (Arnell and Gosling 2016). In addition, the highest number of fatal landslide events (37.8%) occurred in the Black Sea Region, which has rough terrain conditions and high precipitation values. Görüm and Fidan (2021) stated that approximately 72% of these landslides in the Black Sea region occurred due to heavy precipitation, especially in June and July. For example, due to heavy precipitation in 1990, 89 people died in 18 fatal landslides, affecting more than 20 settlements in Trabzon, Rize, Artvin, and Giresun provinces.

The EBSB is also one of the most advantageous basins among the 25 hydrological basins of Türkiye in terms of hydroelectric potential due to its annual total precipitation value and geographical features (Kaygusuz 2018). The average gross energy and technically achievable generation potential of the EBSB are 48,478 (GWh/year) and 24,239 (GWh/year), respectively. This value corresponds to approximately 11% of Türkiye's technically achievable generation potential (Bilgili et al. 2018).

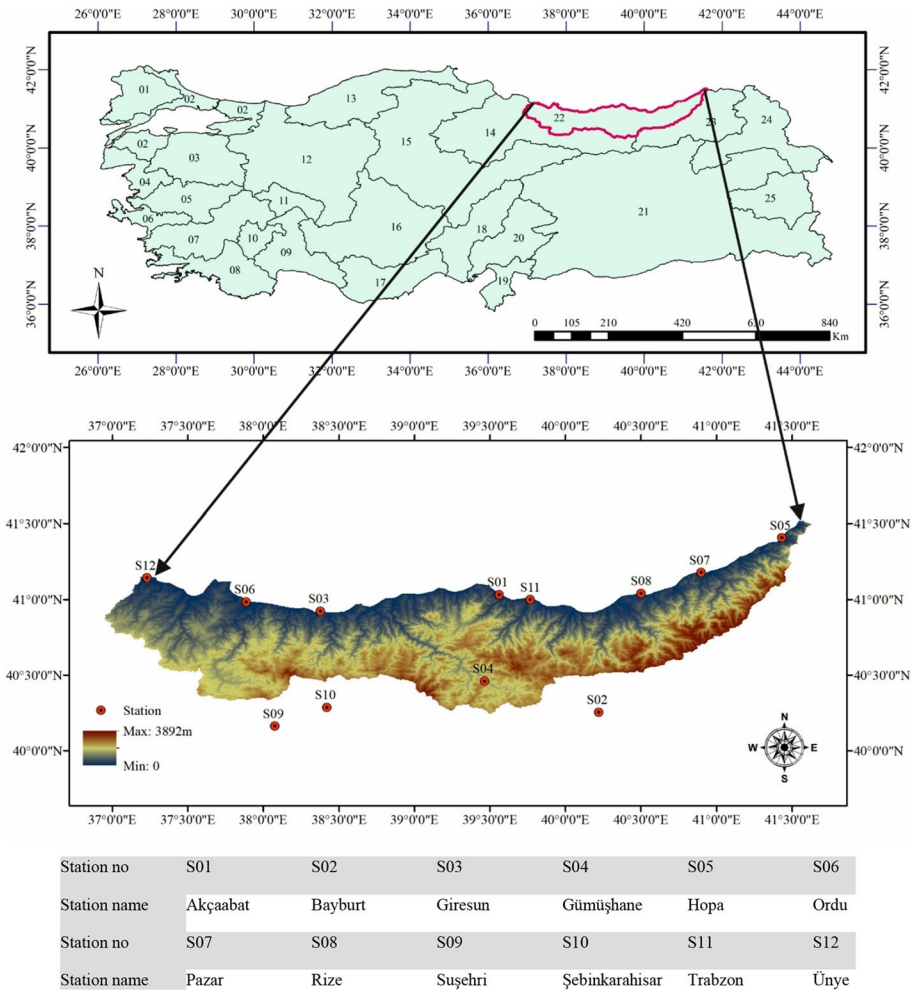


Fig. 2 The locations and names of the meteorological stations used in the study and digital elevation model of the Eastern Black Sea Basin

2.2 Meteorological data set

The historical hydro-meteorological data sets for the EBSB were obtained from the Turkish State Meteorological Service. A considerable time series data was missed in almost all available stations; hence, 12 stations with monthly mean temperature and precipitation data covering 1981–2010 were selected for this study. The locations of these meteorological stations in the basin are given in Fig. 2. Stations within the basin are generally located on the coastline. Four stations were included to represent the mountainous region south of the basin. Bayburt (S02), Suşehri (S09), and Şebinkarahisar (S10) are outside but close to the basin. Basic statistics of observed data for temperature and precipitation variables are given in Tables 1 and 2, respectively.

Table 1 The basic statistics for temperature (°C) observed in the Eastern Black Sea Basin

Station	S01	S02	S03	S04	S05	S06	S07	S08	S09	S10	S11	S12
Minimum	3.1	-11.7	3.5	-6.2	2.0	3.0	2.1	3.1	-7.8	-7.2	3.8	3.2
Mean	14.4	6.9	14.5	9.5	14.4	14.4	13.4	14.3	10.0	9.2	14.7	14.3
Maximum	26.3	22.5	27.0	24.2	28.3	26.7	24.7	27.0	24.8	24.6	27.0	26.9
Standard Dev	6.2	9.0	6.0	8.0	6.1	6.3	6.0	6.3	8.1	8.1	6.1	6.2
Variance	38.5	81.7	36.5	63.8	36.6	39.1	36.2	40.2	65.9	65.4	37.4	38.1

2.3 Reanalysis data set

The ERA-Interim data set is a global atmospheric reanalysis data set covering the period of January 1, 1979 to August 31, 2019. Each grid of the reanalysis data set has a spatial resolution of $0.75^\circ \times 0.75^\circ$. The ECMWF (European Centre for Medium-Range Weather Forecasts) web application server offers a default spatial resolution grid of 0.75° and provides other spatial-resolution grids ranging from 0.125° to 3° based on a bilinear interpolation technique for continuous parameters (Amjad et al. 2020; Liu et al. 2018). The atmospheric variables used in statistical downscaling studies were found to be different from one region to the next. Any atmospheric variable can be used to create statistical downscaling models (Okkan and Fistikoglu 2014). Specifically, atmospheric variables commonly used in downscaling precipitation and temperature, which are available in both reanalysis and GCM data sets, were selected (Araya-Osses et al. 2020; Okkan and Fistikoglu 2014; Okkan and Kirdemir 2016, 2018; Serbes et al. 2019). The large-scale predictors used in the study are given in Table 3.

2.4 General circulation models (GCMs) data set

GCM output data are frequently used in climate change impact studies. Although data from a single GCM can adequately model the current climate, it may not provide sufficiently accurate results in determining the effects of climate change in future periods. For this reason, it is recommended to use more than one GCM output data set in the literature to accurately determine the effects of climate change on different variables in the future and to reveal the sources of uncertainty (Knutti et al. 2010; Araya-Osses et al. 2020). Data belonging to three different GCMs, namely CNRM-CM5.1, HadGEM2-ES, and MPI-ESM-MR, from CMIP5 (5. Climate Model Intercomparison Project) were used in this study. These data sets were also used in dynamic downscaling studies conducted by the Turkish State Meteorological Service and the General Directorate of Water Management. In order to evaluate the findings of this study, care was taken to use common models. While selecting these GCMs, attention has also been paid to the fact that the atmospheric variables in the ERA-Interim reanalysis data set used in the establishment of downscaling models are also included in the historical, RCP4.5, and RCP8.5 scenarios data sets of these GCMs (Araya-Osses et al. 2020; Taylor et al. 2012). The RCP4.5 scenario assumes that the radiative forcing stabilizes in 2100 without exceeding 4.5 W/m^2 (Ouhamdouch and Bahir 2017; Thomson et al. 2011; Wayne 2013). RCP8.5 is the scenario representing the highest emission scenario. According to this scenario, emission values increase as time progresses (Ouhamdouch and Bahir 2017; Riahi et al. 2011). Moreover, the release of greenhouse gases linked

Table 2 The basic statistics for precipitation (mm) observed in the Eastern Black Sea Basin

Station	S01	S02	S03	S04	S05	S06	S07	S08	S09	S10	S11	S12
Minimum	0.0	0.0	0.2	0.0	9.3	2.3	15.3	8.2	0.2	0.0	0.0	1.6
Mean	61.3	38.2	107.2	39.2	188.1	87.4	175.1	189.0	36.4	49.1	70.5	97.5
Maximum	204.0	145.3	521.6	141.9	607.5	251.0	703.2	516.6	162.2	187.0	226.1	298.7
Standard Dev	42.4	27.2	65.3	28.1	110.2	51.4	107.1	105.8	27.5	35.7	44.7	59.1
Variance	1801.8	741.3	4261.2	790.2	12,137.5	2640.3	11,468.9	11,194.4	756.3	1271.3	1996.8	3490.4

Table 3 The large-scale predictors selected from the ERA-Interim reanalysis data set for the calibration of the MARS statistical downscaling model

Atmospheric levels	200 hPa			500 hPa			850 hPa			Surface		
	air200 (°C)	hgt200 (m)	hgt500 (m)	air500 (°C)	air850 (°C)	hgt850 (m)	rhum500 (%)	rhum850 (%)	air (°C)	press (mb)	slp (mb)	prate (kg/m ²)

The air, press, slp, prate, hgt, and rhum represent the mean air temperature, pressure, sea level pressure, precipitation, geopotential height, and relative humidity, respectively

to RCP2.6 has the potential to restrict global warming to a rise of 2 °C or less since the onset of industrialization (Huntingford et al. 2015). In light of this, studying with a stability scenario and a pessimistic scenario would be much more requisite. The large-scale data sets of the historical, RCP4.5, and RCP8.5 scenario outputs of the GCMs decided to be used in the study were accessed from the Earth System Grid Federation website.

3 Methods

3.1 Multivariate adaptive regression splines (MARS)

One of the most fundamental problems in engineering science is developing an equation that can predict a dependent variable using one or more independent variables. Many researchers are involved in mathematics, statistics, computer science, and engineering to solve this problem. The primary purpose of these studies is to obtain a function (f) that can predict a variable (y) using one or more (x_1, x_2, \dots, x_n) predictors. MARS, developed by Friedman (1991), is a multivariate non-parametric regression method for flexible regression modeling high dimensional data. The difference between this method and other methods is that it overcomes the limitations of the methodologies stated by Friedman (1991). One of the most robust features of this method is that it provides an extremely general regression equation while avoiding overfitting. The MARS method can process a wide range of nested predictor types and naturally combine them without removing the missing data from the data set (Friedman and Roosen 1995). In the MARS method, instead of assuming the relationship between dependent and independent variables, there is an approach to revealing this relationship using the divide and conquer strategy (Zhang and Goh 2016). This strategy divides the training data set to establish the downscaling model into multi-part linear sections called splines. Endpoints of linear segments with multiple parts are defined as knots, and linear segments between these nodes are defined as basic functions (Suman et al. 2016). Setting up a MARS-based downscaling model involves a forward and backward process. In the forward process, the model is created by iteratively selecting the best pairs of basic functions that increase the model's accuracy. However, the excess of selected basis functions in this process may create a complex and overfitted model with low predictive ability against new data. To increase the prediction capability of this model, the second stage, or, in other words, the backward process, is started. The model is pruned in this process by removing the ineffective basis functions (Khuntia et al. 2015; Samui 2013; Tiryaki et al. 2019).

MARS is built on basic functions defined by the following equations:

$$|x - t|_+ = \max(0, x - t) = \begin{cases} x - t & \text{if } x > t \\ 0 & \text{otherwise} \end{cases} \quad (1)$$

$$|t - x|_+ = \max(0, t - x) = \begin{cases} t - x & \text{if } x < t \\ 0 & \text{otherwise} \end{cases} \quad (2)$$

where t represents the “knots”. The formulations are the basic functions predicting function Y (Dey and Das 2016). The general MARS model equation can be defined as follows:

$$y = \beta_0 + \sum_{m=1}^M \beta_m \times bf_m(x) \quad y = \beta_0 + \sum_{m=1}^M \beta_m \times bf_m(x) \tag{3}$$

where y is the output variable, M is the number of basic functions included in the model, β_0 is the constant term, $bf_m(x)$ is the m 'th basic function that may be a single spline function or an interaction of two or more spline functions, β_m is the coefficient of the m 'th basic function (Khuntia et al. 2015; Tiryaki et al. 2019). More detailed information about the MARS statistical downscaling method and its applications can be found in Friedman (1991).

This study used the MARS method to obtain an equation to estimate monthly average temperature and monthly total precipitation data from meteorology stations using coarse-resolution atmospheric variables. The above analyses were performed using the Salford Predictive Modeler 8.0 software.

3.2 Quantile delta mapping bias correction

It is stated in the literature that the downscaling model outputs can contain some bias. This bias may be caused by different reasons, such as the resolution of the GCMs used in downscaling, the selection of the estimators in the reanalysis data set, the downscaling method, and the period to be projected (Okkan and Inan 2015b). Due to the different sources of these biases, it is not easy to resolve them within climate models. Therefore, these biases must be corrected after obtaining downscaling model outputs (Kim et al. 2020). Many studies have been carried out in which different bias correction methods are applied to correct the bias as mentioned above and to make future climate data more realistic (Guo et al. 2019; Kim et al. 2020; Okkan and Inan 2015b; Reiter et al. 2018; Salmani-Dehaghi and Samani 2021; Zhao et al. 2017; Okkan et al. 2023). This study used the quantile delta mapping (QDM) method for bias correction. QDM was developed to preserve the relative change ratio in the modeled quantiles of variables (Cannon et al. 2015; Kim et al. 2020). The basic equation of the QDM method is given in Eq. (4). This equation includes the bias-corrected value term obtained using the observation data and the relative change term (Δ) obtained from the model outputs.

$$\hat{X}_{m,p}(t) = \hat{X}_{o:m,h;p}(t) \cdot \Delta_m(t) \tag{4}$$

$$\hat{X}_{o:m,h;p}(t) = F_{o,h}^{-1} \left[F_{m,p}^{-1} \{ X_{m,p}(t) \} \right] \tag{5}$$

$$\Delta_m(t) = \frac{X_{m,p}(t)}{F_{m,h}^{-1} \left[F_{m,p}^{(t)} \{ X_{m,p}(t) \} \right]} \tag{6}$$

where $\hat{X}_{m,p}(t)$ is the model (simulated) data at time t of the projected period, $\Delta_m(t)$ is the relative change in the model data between the historical and future periods, $F_{m,p}^{-1}$ and $F_{o,h}^{-1}$ are the cumulative probability function (CDF) of the raw data of the statistical downscale model and the inverse CDF of the observed data, and $\hat{X}_{o:m,h;p}(t)$ is the bias-corrected data for the historical period, respectively. Thus, the bias-corrected future projection at time t is given by multiplying the relative change $\Delta_m(t)$ by the historical bias-corrected value (Kim

et al. (2020). More details about the QDM and its implementation can be found in Cannon et al. (2015), Kim et al. (2020), and Okkan et al. (2023).

3.3 Model evaluation statistics

To evaluate the MARS-based downscaling model performance concerning the observed precipitation and temperature data, four statistical performance indices, namely the root mean square error (RMSE), scatter index (SI), mean absolute error (MAE), and Nash–Sutcliffe (NS), were used. These indices are used primarily to assess the performance of statistical downscaling models (Al-Mukhtar and Qasim 2019; Okkan and Inan 2015a, b). Moriasi et al. (2007) also emphasized the importance of using RMSE and NS statistical performance indices for evaluating model performances in hydrological studies. The indices mentioned above are computed from Eqs. (7–10).

$$RMSE = \sqrt{\frac{1}{n} \sum_{i=1}^n (X_{o,t} - X_{m,t})^2} \quad (7)$$

$$SI = \frac{RMSE}{\overline{X_{o,t}}} \quad (8)$$

$$MAE = \frac{1}{n} \sum_{t=1}^n |X_{o,t} - X_{m,t}| \quad (9)$$

$$NS = 1 - \left[\frac{\sum_{t=1}^n (X_{o,t} - X_{m,t})^2}{\sum_{t=1}^n (X_{o,t} - \overline{X_{o,t}})^2} \right] \quad (10)$$

where X_o is the observed value, X_m is the downscaled value, and $\overline{X_o}$ is the mean value. The RMSE, SI, and MAE statistics are among the error-index types used to evaluate the estimation performances of the models. The closer the values of these statistics are to the zero value, the higher the model performance (Singh et al. 2005). The NS statistic is a dimensionless model performance statistic (Al-Mukhtar and Qasim 2019; Moriasi et al. 2007). A value of NS close to 1 indicates that the model is efficient (Okkan and Inan 2015b). General performance ratings of the NS were presented by Moriasi et al. (2007).

3.4 Model development applications

To assess the efficacy of statistical downscaling models, the observed data sets and ERA-Interim atmospheric variables were initially partitioned into two distinct groups: training and testing. The data for the 1981–2004 (80%) period were used to train the statistical downscaling models, and the remaining data for the 2005–2010 (20%) period were used to test the models. The flowchart of the proposed downscaling strategy is summarized in Fig. 3.

The flowchart shows that the time series of large-scale ERA-Interim predictors and precipitation and temperature variables observed from stations were standardized before being

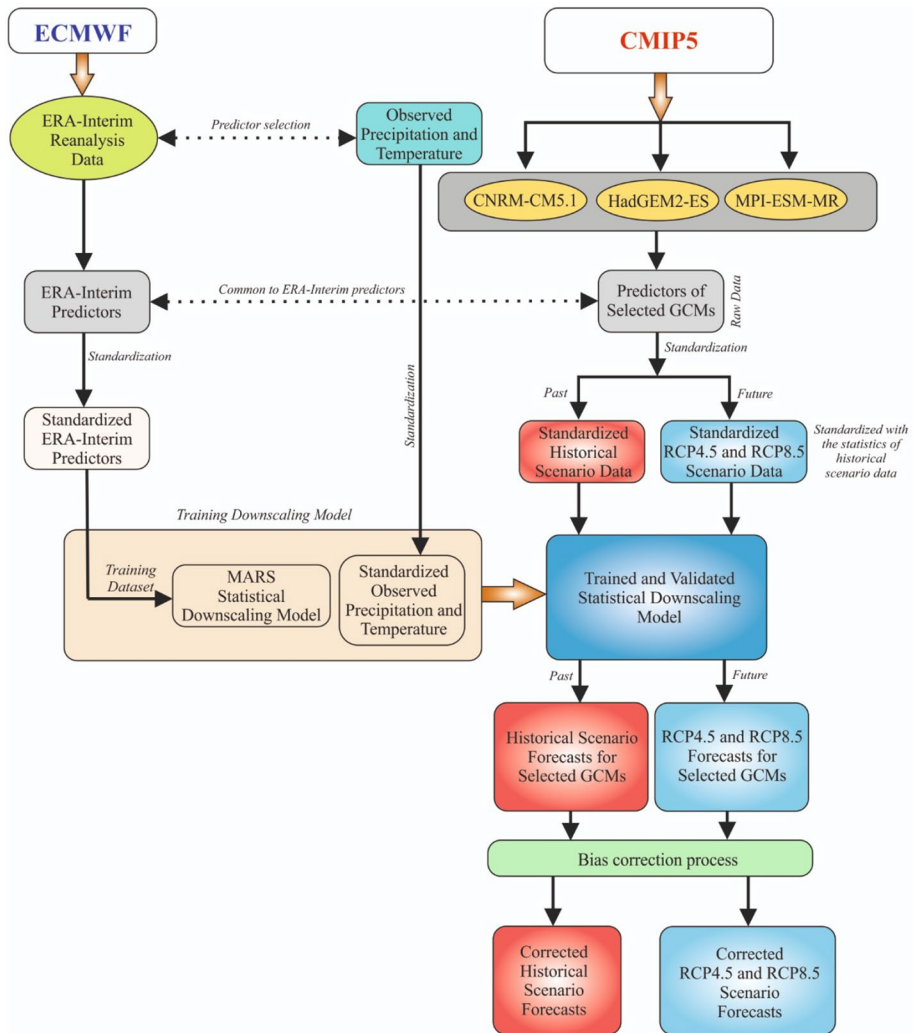


Fig. 3 Flow chart of the statistical downscaling strategy applied in the study

presented to MARS-based downscaling models. Standardization is a simple and convenient bias correction method proposed by Pan and Van Den Dool (1998) that is applied to data sets before being presented to downscaling models. Wilby et al. (2004) also emphasized that the standardization procedure is applied before the data is downscaled to reduce biases in the mean and variance of the GCM data. Therefore, scenario data of GCMs are also standardized before being downscaled. The approach suggested by Wilby et al. (2004) was used for the standardization procedure. Selecting the constraints in the MARS method is important for model performance. The optimum values for each constraint were determined separately for each station by trial and error. Once the training phase of the MARS-based downscaling models for temperature and precipitation variables was accomplished, these models were evaluated using the testing data set. NS performance statistics, including RMSE, SI, and MAE, were employed to assess the models' performances.

3.5 Trend analysis

Linear regression, moving average, and filtering are some approaches for trend detection in time series. On the other hand, non-parametric trend studies are less susceptible to outliers and independent of key assumptions like linearity and normality (Zhang et al. 2010). Furthermore, non-parametric trend tests have better power for hydrological time series with skewed probability distributions (Önöz and Bayazit 2003). Mann–Kendall (MK) is often preferred in the literature to evaluate monotonic trends in hydro-meteorological time series, and the World Meteorological Organization recommends its use (Kumar et al. 2009; Tongal 2019). However, since the MK is affected by serial correlation, the modified MK by Hamed and Rao (1998) is used in this trend study. The literature thoroughly describes this procedure (Achite et al. 2023; Sonali and Kumar 2013; Zhang et al. 2010). In addition, the innovative trend analysis (ITA) with significance test (ITST) proposed by Şen (2017), which does not contain any assumptions for determining ITA’s monotonic trends and is based on graphical and trend detection in different level groups (Şen 2012), was also used.

In addition to monotonic trends, analyzing the trends of low and high values that trigger drought and flood events enables effective water resources management. To achieve this goal, ITA is proposed by Şen (2012), which provides a visual-linguistic interpretation that does not require any assumptions. However, the definition of low and high values in ITA is fuzzy, as it can vary from person to person. Improved visualization of innovative trend analysis (IV-ITA) was proposed by Güçlü (2020) for the objective separation of low and high values to overcome this deficiency. According to this method, the time series is divided into two in the center and sorted from lowest to highest. The sequence number is placed on the horizontal axis, and both series are placed vertically according to the sequence number (Fig. 4). The difference series is formed by subtracting the values of the first series from the values of the second series according to the sequence number. Then, the change point is determined by applying the Pettitt test (Pettitt 1979) to the difference series. The right side of the change point of the difference

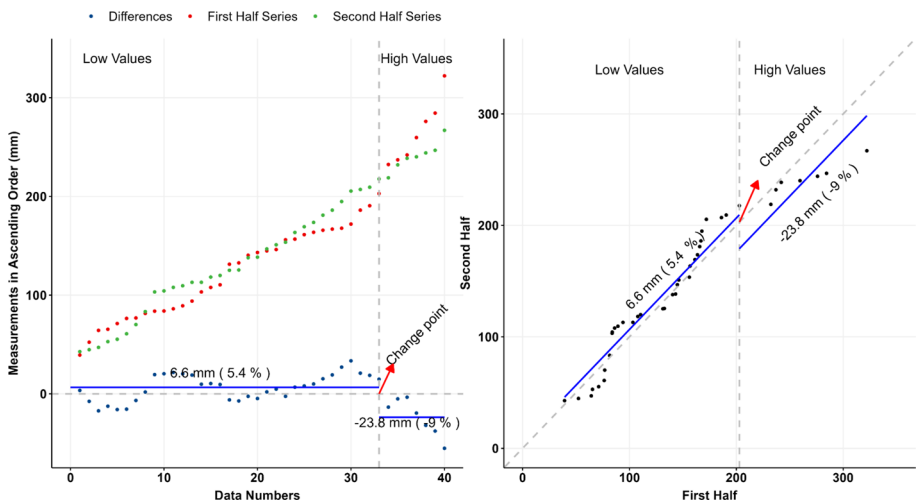


Fig. 4 Illustration of **a** IV-ITA and **b** classical ITA method (Körük et al. 2023)

Table 4 Performance statistics of statistical downscaling models established for the temperature

Data set Stations	Performance statistics for the training data set				Performance statistics for the testing data set			
	RMSE (°C)	SI	MAE (°C)	NS	RMSE (°C)	SI	MAE (°C)	NS
S01	0.440	0.031	0.345	0.995	0.571	0.037	0.470	0.992
S02	0.723	0.108	0.538	0.994	0.760	0.099	0.600	0.993
S03	0.474	0.033	0.367	0.994	0.877	0.058	0.628	0.979
S04	0.503	0.054	0.407	0.996	0.591	0.058	0.461	0.995
S05	0.768	0.054	0.565	0.983	1.210	0.080	0.894	0.967
S06	0.384	0.027	0.307	0.996	0.533	0.035	0.443	0.993
S07	0.446	0.034	0.346	0.994	0.498	0.035	0.400	0.993
S08	0.389	0.028	0.308	0.996	0.452	0.030	0.371	0.995
S09	0.518	0.053	0.391	0.996	0.602	0.056	0.476	0.995
S10	0.555	0.062	0.433	0.995	0.591	0.058	0.456	0.995
S11	0.426	0.029	0.334	0.995	0.436	0.028	0.350	0.995
S12	0.427	0.030	0.335	0.995	0.630	0.042	0.495	0.990

series shows the change of high values, and the left side shows the change of low values. If the difference values for both sides accumulate above the horizontal axis, it means an increasing trend, and if they accumulate below it, it means a decreasing trend. However, there is no trend if these accumulate around the horizontal axis. The percentage change of the group of low values is calculated as $100 \times (\text{average of the difference series on the left-hand side}) / (\text{average of the sorted first half})$. The percentage change of the group of high values is calculated as $100 \times (\text{average of the difference series on the right-hand side}) / (\text{average of the sorted second half})$.

4 Results and discussion

4.1 Training and testing of statistical downscaling model

Performance statistics for the training and testing data sets for temperature and precipitation variables are given in Tables 4 and 5, respectively. NS performance statistics vary between 0.983–0.996 and 0.967–0.995 for training and testing data sets, respectively (Table 4). The models for all stations are in the *very good* class, according to Moriasi et al. (2007). In addition, the models of all stations give very similar results for the temperature variable. Since it will be challenging to provide results for all stations in terms of presentation, only the time series plots and scatter plots of the temperature prediction of training and testing data sets in Hopa and Suşehri stations are given. The EBSB shows two different climatic characteristics: humid climates on the coast and continental climates inland. Therefore, the time series and scatter plots of temperature predictions at Suşehri station in the interior region and Hopa station in the coastal region are representative examples (Fig. 5).

The performance values calculated for the precipitation variable are lower than those calculated for the temperature variable (Table 5). For the precipitation variables, it is seen that the values of RMSE, SI, MAE, and NSE performance statistics vary between

Table 5 Performance statistics of statistical downscaling models established for the precipitation

Data set Station	Performance statistics for the training data set				Performance statistics for the testing data set			
	RMSE (mm)	SI	MAE (mm)	NS	RMSE (mm)	SI	MAE (mm)	NS
S01	28.186	0.457	21.845	0.568	24.966	0.419	19.952	0.621
S02	16.633	0.446	12.929	0.619	19.260	0.458	14.539	0.529
S03	37.542	0.353	28.100	0.609	58.500	0.528	35.174	0.501
S04	15.641	0.411	12.227	0.671	18.474	0.423	14.443	0.642
S05	64.816	0.346	48.092	0.639	67.295	0.352	51.411	0.680
S06	31.777	0.367	24.026	0.609	32.019	0.355	25.338	0.641
S07	64.879	0.376	47.180	0.628	58.227	0.314	48.100	0.717
S08	61.446	0.330	47.728	0.656	62.511	0.313	50.159	0.671
S09	16.706	0.461	12.232	0.641	16.198	0.434	12.998	0.609
S10	20.041	0.407	15.042	0.698	15.172	0.311	12.398	0.777
S11	30.784	0.434	22.954	0.513	26.438	0.382	20.488	0.682
S12	37.314	0.391	27.224	0.588	45.177	0.427	32.419	0.470

15.641–64.879 mm, 0.330–0.461, 12.227–48.092 mm, and 0.513–0.698 for the training data set, respectively. For the testing data set, the RMSE, SI, MAE, and NSE performance statistics range between 15.172–67.295 mm, 0.311–0.528, 12.398–51.411 mm, and 0.470–0.777, respectively. When the calculated NS performance statistics values were evaluated, the models of Gümüşhane, Rize, and Şebinkarahisar stations were in the *good* class for the training data set. The other stations were in the *satisfactory* class. For the testing data set, it was determined that only the model belonging to the Ünye station was in the *unsatisfactory* class, while the models belonging to Hopa, Pazar, Rize, Şebinkarahisar, and Trabzon stations were in a *good* class, and the other stations were in the *satisfactory* class. When the calculated performance statistics were evaluated in general, it was seen that the statistical downscaling models established for the precipitation variable gave satisfactory results for the whole basin except Ünye station. As a representative example, both time-series and scatter plots of precipitation predictions at Şebinkarahisar and Ünye stations are presented in Fig. 6 for both periods.

Although the MARS-based statistical downscaling model results at all stations for the temperature variable are in the *very good* class, it is impossible to say the same for the precipitation variable. Al-Mukhtar and Qasim (2019), Hassan et al. (2014), and Yang et al. (2012) have demonstrated that downscaling can better reproduce temperature series than precipitation. This is thought to be because the dispersion of precipitation data is greater than the temperature parameter. Although MARS-based downscaling models gave consistent results in almost all stations in and around the basin, their performance in estimating extreme values was limited, especially for some stations on the coastline. In the study of Okkan and Kirdemir (2016), it was stated that this situation is highly possible. Also, Tripathi et al. (2006) stated in their study that statistical models might not explain all the variance of the modeled variable.

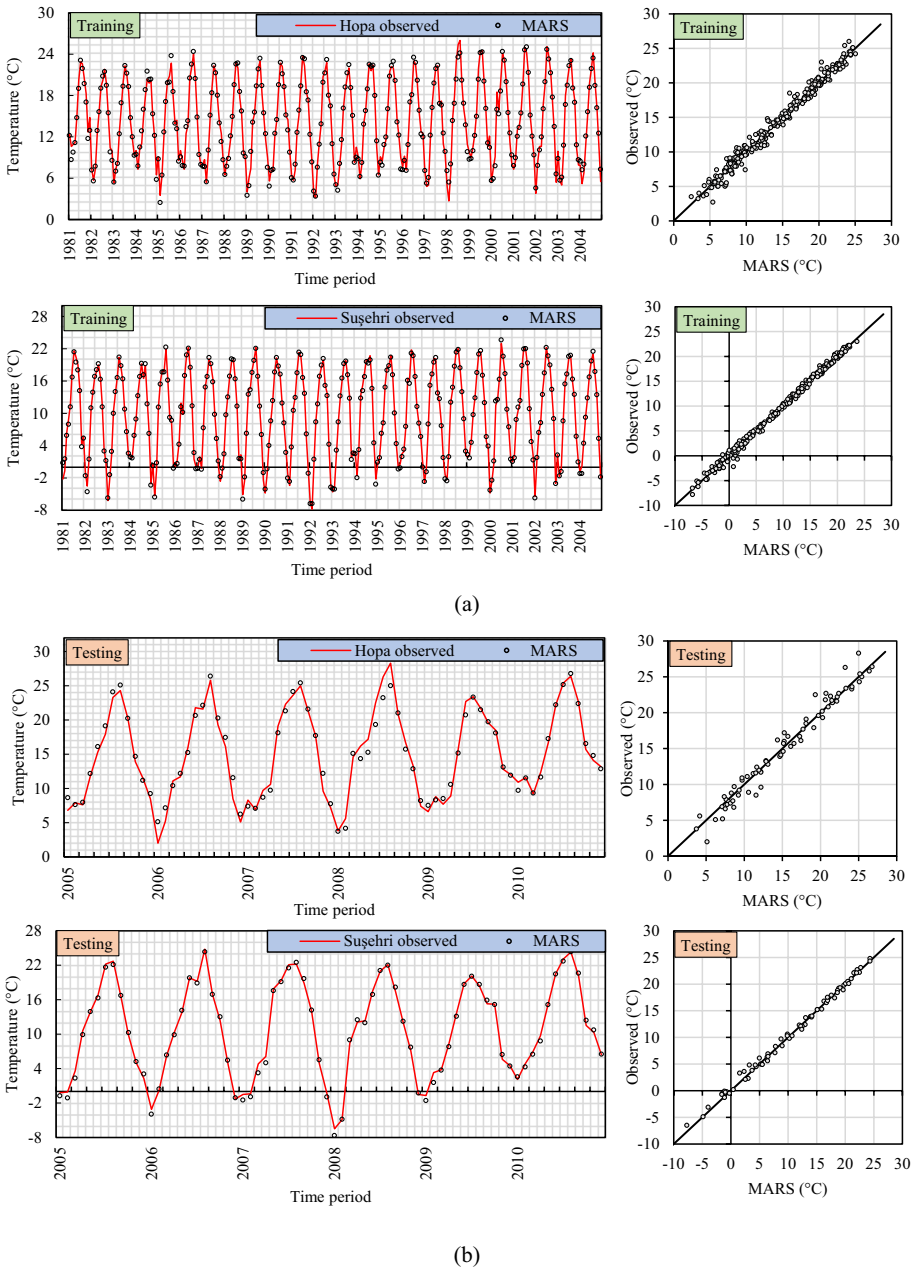


Fig. 5 Temperature predictions of Hopa and Suşehri stations derived from the MARS statistical downscaling model for the **a** training and **b** testing data sets

4.2 Downscaling outputs of three GCMs

In the previous section, the highest-performance MARS-based statistical downscaling models that estimate local scale temperature and precipitation variables using large-scale

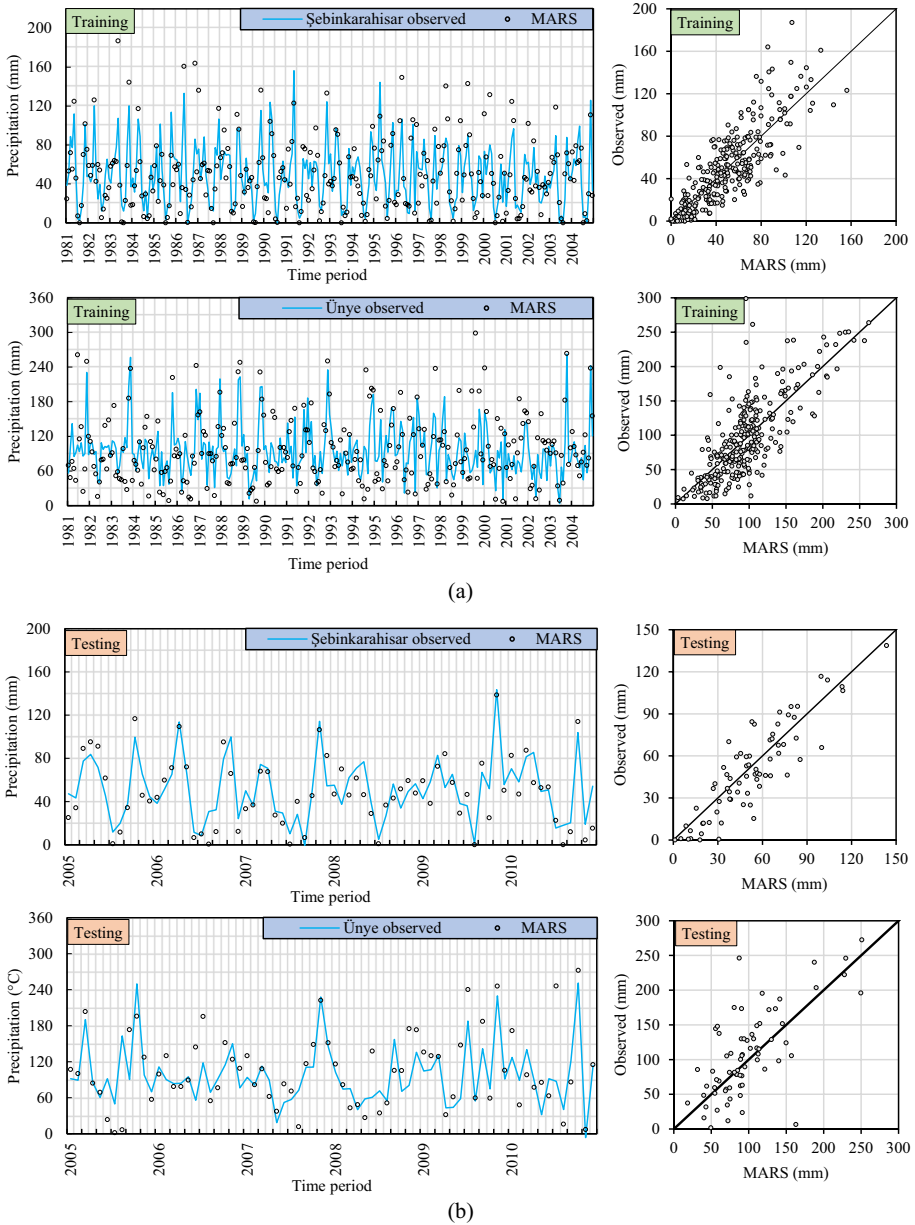


Fig. 6 Precipitation predictions of Şebinkarahisar and Ünye stations derived from the MARS statistical downscaling model for the **a** training and **b** testing data sets

atmospheric variables were determined for all stations. After that, the large-scale atmospheric predictors in the historical, RCP4.5, and RCP8.5 data sets were arranged for the basin, and then the standardization procedure was applied. As can be seen in Fig. 3, RCP

data were standardized using historical scenario data. These standardized large-scale predictor data sets were used as new inputs for statistical downscaling models established using large-scale atmospheric predictors in the ERA-Interim reanalysis data set. Thus, a standardized time series of temperature and precipitation variables for each GCM was produced for each station and past and future scenarios. Standardized temperature and precipitation data obtained from the MARS-based statistical downscaling models were converted into units by restandardization.

A bias correction technique was used to obtain the temperature and precipitation time series to lessen possible biases in MARS-based forecasts. The obtained MARS statistical downscaling model outputs may contain different biases depending on the GCM resolutions, atmospheric variables, downscaling technique, and the period in which the data is generated (Kang and Moon 2017; Okkan and Kirdemir 2016). Chen et al. (2011) and Sachindra et al. (2014) have also emphasized that correcting biases is required before using projections in climate impact studies. After the bias correction procedure, past and future temperature and precipitation data were evaluated separately for 1980–2005, 2021–2050, 2051–2080, and 2081–2100, respectively.

To be able to say whether the GCM data produced under different scenarios for future periods and downscaled to the local scale are close to the real values, it is necessary to determine whether these data sets accurately represent the climatic conditions of the past period (Dibike et al. 2008; Okkan and Kirdemir 2016). Therefore, the basic statistics (mean, maximum, minimum, and standard deviation) of the bias-corrected and uncorrected historical scenario outputs representing the period 1980–2005 and the basic statistics of the temperature and precipitation variables of the observation data for the same period were compared for all stations. However, the tables for the Akçaabat station are only given due to the page limitation (Tables 6, 7).

All statistics for the variable temperature approach and the observation values, especially the monthly average values, are the same as for all three GCMs (Table 7). In this case, it is thought that the outputs of the RCP4.5 and RCP8.5 scenarios, which are the future optimistic and pessimistic scenarios of GCMs, may more accurately represent the possible changes in the temperature values of the region.

As in the temperature variable, the bias correction procedure brings the values of the model outputs closer to the observation values (Table 7). After the bias correction procedure, it is seen that the monthly average precipitation values and the maximum precipitation values, which are essential for the region due to floods, are close to the observation values.

In general, it has been determined that the outputs of all GCMs for temperature and precipitation variables have values close to the observation data for the base period. Therefore, using these GCMs to generate future period data is considered plausible as it may yield realistic results. In addition, a similar evaluation was performed by Gebre and Ludwig (2015). Subsequently, the mean temperature and monthly precipitation of 12 meteorology stations strategically proximity of the EBSB were projected under RCP4.5 and RCP8.5 scenarios for the three future decades (2021–2050, 2051–2080, and 2081–2100). Foreseen changes in the future for temperature and precipitation variables were evaluated separately.

Table 6 Comparison of the basic statistics of the observation data of the Akçaabat station (S01) temperature variable for the period of 1980–2005 with the statistics of the bias-corrected and uncorrected GCM historical scenario data

Month	Jan	Feb	Mar	Apr	May	Jun	Jul	Aug	Sep	Oct	Nov	Dec
<i>Observed</i>												
Mean (°C)	7	6.3	7.6	11.2	15.3	20	23	23.2	20	16.1	11.5	8.7
Maximum (°C)	9.2	8.6	10.6	14.4	17.1	21.3	25.3	25.1	22	18.2	13.6	12.5
Minimum (°C)	3.8	3.1	4.9	8.8	13.7	19	20.5	20.6	17.7	14	8.2	6
Standard Dev (°C)	1.7	1.5	1.4	1.4	0.9	0.6	1.1	1	1	1.1	1.3	1.6
<i>CNRM historical</i>												
Mean (°C)	6	6.5	9	11.4	13.9	18.5	23.4	24.1	21.2	17.2	12.2	8.1
Maximum (°C)	9	9.5	11.5	12.7	15.2	22.9	27.4	27.3	23.2	18.9	14.7	10.5
Minimum (°C)	2.2	4.2	6.8	9.7	12.8	14.9	21.2	22.6	20	13	8.9	2.6
Standard Dev (°C)	1.7	1.5	1.3	0.7	0.7	1.8	1.2	1.3	1	1.1	1.8	1.6
<i>CNRM historical bias corrected</i>												
Mean (°C)	7	6.3	7.6	11.2	15.3	20	23	23.2	20	16.1	11.5	8.7
Maximum (°C)	9.9	9.2	10.3	13.8	17.1	21.6	26.9	25.8	22.1	17.7	13.4	11.1
Minimum (°C)	3.4	4.1	5.2	7.8	13.9	18.8	20.9	22	18.8	11.9	9.2	3
Standard Dev (°C)	1.7	1.5	1.4	1.4	0.9	0.6	1.1	1	1	1.1	1.3	1.6
<i>HadGEM historical</i>												
Mean (°C)	5.1	6.3	9.5	13.7	18.4	21	22.6	21.7	18.8	16.8	10.8	7.1
Maximum (°C)	9.4	9	12.3	15.9	21.7	23.9	25.1	23.9	20.6	18.8	14	10.1
Minimum (°C)	−0	2.7	5.6	10.8	15.3	19.5	19.6	20.1	16.5	14	7.4	3.4
Standard Dev (°C)	2	1.7	1.6	1.3	1.3	1	1.4	1.1	1.1	1.2	1.7	1.7
<i>HadGEM historical bias corrected</i>												
Mean (°C)	7	6.3	7.6	11.2	15.3	20	23	23.2	20	16.1	11.5	8.7
Maximum (°C)	11	8.7	10.1	13.6	17.5	21.7	25.1	25.3	21.7	17.9	14	11.5
Minimum (°C)	2.7	3.1	4.1	8.1	13.3	19	20.5	21.6	17.8	13.5	8.9	5.3
Standard Dev (°C)	1.7	1.5	1.4	1.4	0.9	0.6	1.1	1	1	1.1	1.3	1.6
<i>MPI historical</i>												
Mean (°C)	4.6	6.8	9.9	15.2	16.6	19.5	21.5	22.8	20.9	15.8	11.4	6.6
Maximum (°C)	6.8	10.8	14.4	18	18.6	21.3	24	25.1	24.9	19.1	14.4	9.2
Minimum (°C)	0.9	0.4	6.2	10.5	14.8	17	18.7	19.4	16.7	12.5	7.9	2.6
Standard Dev (°C)	1.6	2.3	2.2	1.9	1.2	1.2	1.2	1.5	1.9	1.6	1.8	1.3
<i>MPI historical bias corrected</i>												
Mean (°C)	7	6.3	7.6	11.2	15.3	20	23	23.2	20	16.1	11.5	8.7
Maximum (°C)	9.3	9	10.6	13.2	16.8	20.9	25.2	24.9	22.2	18.4	13.7	11.8
Minimum (°C)	3.1	2.2	5.2	7.7	14	18.7	20.5	20.9	17.7	13.8	9.1	3.8
Standard Dev (°C)	1.7	1.5	1.4	1.4	0.9	0.6	1.1	1	1	1.1	1.3	1.6

4.2.1 Foreseen changes in future temperature

The bias-corrected outputs of three different GCMs from RCP4.5 and RCP8.5 scenarios were compared with the bias-corrected historical scenario outputs of the same GCMs to evaluate the foreseen temperature increases in three periods in the future (Fig. 7).

Table 7 Comparison of the basic statistics of the observation data of the Akçaabat station (S01) precipitation variable for the period of 1980–2005 with the statistics of the bias-corrected and uncorrected GCM historical scenario data

Month	Jan	Feb	Mar	Apr	May	Jun	Jul	Aug	Sep	Oct	Now	Dec
<i>Observed</i>												
Mean (mm)	76.6	64.6	51	48.8	42.7	48.1	25.1	40.6	55.5	113.3	97.9	76.3
Maximum (mm)	203.5	192.2	96.1	89.1	69.1	90.4	78	88.8	154	204	189.4	191
Minimum (mm)	9.8	26.4	9.7	19.1	9.8	7.9	2.6	9.6	3.2	35.5	4.7	18.2
Standard Dev (mm)	53.8	40.4	20.7	20.7	15.9	21.8	17.4	21.6	32.6	48.7	52.8	45.5
<i>CNRM historical</i>												
Mean (mm)	85.3	65.4	57.7	51.2	48.4	40.9	35.1	37.6	57.2	85.1	87.6	92.4
Maximum (mm)	150.1	98.9	89.4	88.9	62.1	52.7	46.2	121.6	106	195	128.9	245.6
Minimum (mm)	49.2	39.7	42.1	36.1	32.6	29.9	16.8	24.6	39.2	48.5	37	34.4
Standard Dev (mm)	27.2	17.1	12.2	10.7	7.7	6.1	6.7	18.3	15.3	30.8	28.3	50.8
<i>CNRM historical bias corrected</i>												
Mean (mm)	76.2	64.4	50.9	48.6	42.7	48	25.1	40.4	55	113.1	98	76.2
Maximum (mm)	221.8	151.4	109.9	133.5	72.8	93.8	56.9	142.3	179	293.8	176.3	216
Minimum (mm)	16.9	14.7	26.1	22	14.7	15.4	0.4	25.2	20.6	56.7	18.5	25.3
Standard Dev (mm)	54.8	40.5	21.6	22.3	15.4	21.6	15	22.1	36.1	49.5	50.4	45.8
<i>HadGEM historical</i>												
Mean (mm)	76.3	72.5	65.1	53.6	47	38.6	22.7	33.2	62.8	77	97.5	82
Maximum (mm)	128.6	121.9	96.4	73.1	55.9	43.6	36.6	45.5	82.2	139.2	180.3	175.2
Minimum (mm)	0.1	47.3	48.3	41.4	39.1	32.5	0.1	12.2	45.6	39.6	0.1	48.4
Standard Dev (mm)	27.5	18.7	12.1	7.5	4.5	2.9	10.3	6.7	10	29.3	41.2	31.6
<i>HadGEM historical bias corrected</i>												
Mean (mm)	77.2	64.1	50.9	48.7	42.7	48	25.7	40.7	55.3	113.2	98.4	76
Maximum (mm)	185.8	189.9	110.9	111.2	77.5	88.9	48.6	83.4	127	218.2	206.9	223.6
Minimum (mm)	0	18	24.4	19.7	18.6	13	0	1	12.1	52.3	0	30.3
Standard Dev (mm)	47.7	43.5	21.1	21.3	16.2	21.1	14.4	18.3	31.6	48.8	50.4	46.6
<i>MPI historical</i>												
Mean (mm)	100.9	62.2	56.1	44.4	51.1	50.3	41.4	39.8	52.9	80.6	71.4	133.4
Maximum (mm)	353.4	111.7	90.8	62	76.3	86.3	56.9	56.5	97.1	112.3	103.4	285.7
Minimum (mm)	44.5	33.4	33.7	23.2	39.1	36.9	30.3	25.8	34.4	46.2	51.8	48.5
Standard Dev (mm)	62.8	16.9	13.5	8.6	9.6	10.8	7.8	7.2	16	17.2	16.2	72
<i>MPI historical bias corrected</i>												
Mean (mm)	76.1	64.1	50.9	48.9	42.6	47.9	25	40.5	55.1	113.3	97.5	76.2
Maximum (mm)	300.9	205.7	108.1	94.9	88.6	133.4	65.1	98	157	208.3	211.9	173.8
Minimum (mm)	29.1	10.7	19.9	9	23.8	22.7	5.5	8.3	20.9	31.4	39.5	24
Standard Dev (mm)	55.2	43.2	21.3	19.3	16.7	23.4	17.4	21.6	34.8	47	53.7	45.7

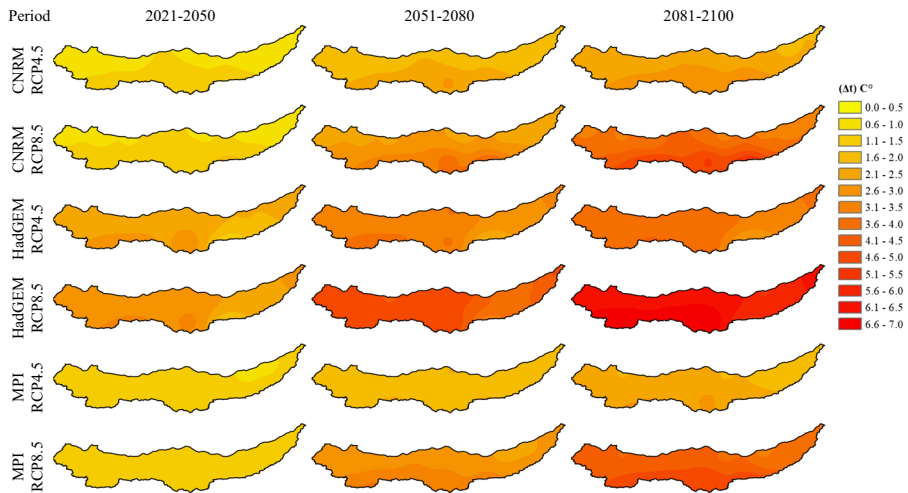


Fig. 8 Spatial distribution for the change of annual average temperature (compared to base period) in future periods under RCP4.5 and RCP8.5 scenarios

It is foreseen that the temperature increases will reach up to 10 °C, especially in the summer months. Also, the increases in the projected temperature values according to the RCP8.5 scenario outputs were higher than the RCP4.5 scenario outputs. The spatial distribution for the future changes in annual mean temperature and precipitation of the EBSB (compared to the base period) under scenarios RCP4.5 and RCP8.5 was built by the inverse distance-weighted interpolation technique with the ArcGIS 10.5 software. Maps showing the spatial distribution of projected changes in annual mean temperatures are given in Fig. 8.

When the maps showing the changes in the annual average temperature values were examined, it was seen that there were temperature increases in all three periods of the future. Increases were between 0.5 and 4 °C in 2021–2050 and 6 °C in 2051–2080. It was observed that the highest temperature increase occurred around 7 °C at the end of the century. While the highest temperature increase was obtained from the HadGEM model outputs, the least was obtained from the MPI model outputs. In large-scale studies covering the basin (Bağçacı et al. 2021; Turkes et al. 2020), similar findings suggest that it is also projected to increase up to 6 °C towards the end of the century, especially since the intensity of the increase is very high for summer and autumn. It was observed that the temperature increases were most concentrated in the stations located in the regions with continental climates in the south of the basin. In arid areas like the interior part of the EBSB, positive changes in temperature will undoubtedly accelerate the desertification process, ultimately affecting agricultural activities in the basin (Abbasnia et al. 2016; Al-Mukhtar and Qasim 2019). In addition, Schroerer and Kirchengast (2018) state that a warmer atmosphere can hold more water vapor, producing more intense precipitation, including precipitation intensity increases of 6–7% per degree of warming or even more for sub-hourly precipitation (Araya-Osses et al. 2020).

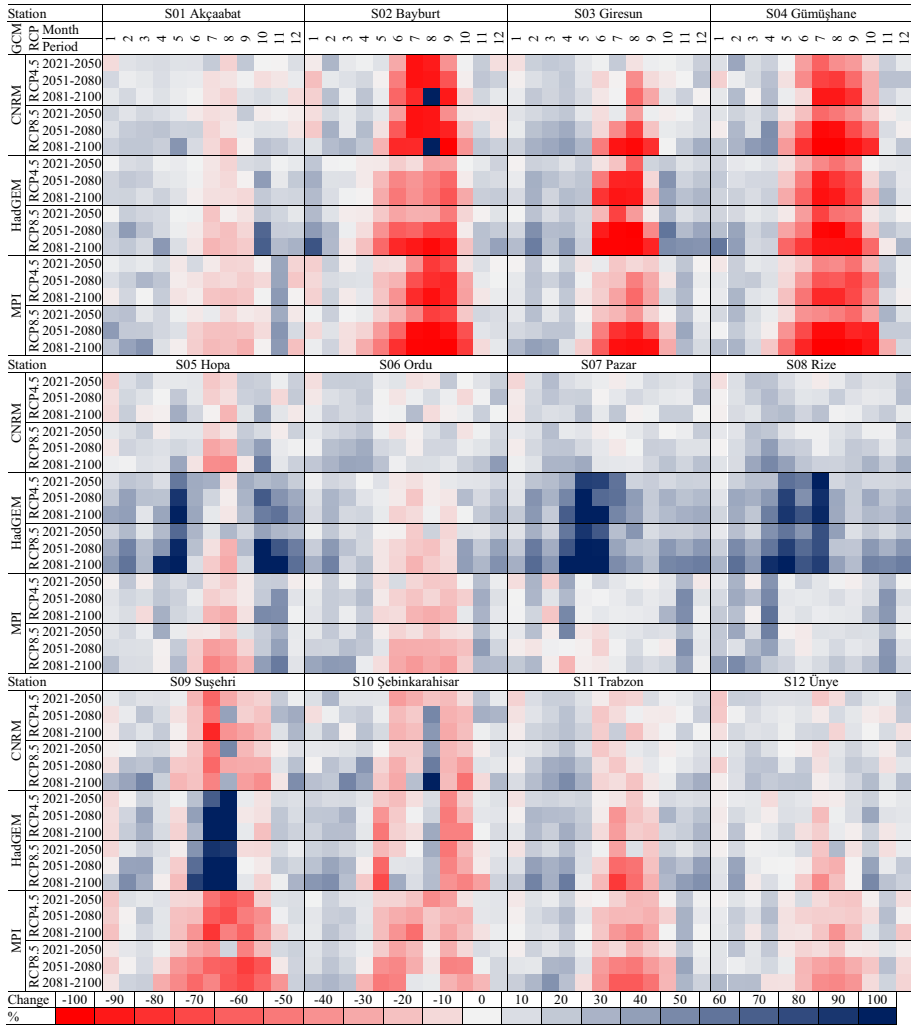


Fig. 9 Precipitation (%) changes about the 1980–2005 historical scenario period for RCP4.5 and RCP8.5 scenarios

4.2.2 Foreseen changes in future precipitation

The relative changes (%) of monthly mean precipitation (compared to the base period 1981–2005) in the EBSB under RCP4.5 and RCP8.5 scenarios are shown in Fig. 9.

The results obtained for the monthly mean precipitation show more spatial variability and less robustness compared to the temperature variable. The changes in seasonal mean precipitation in the EBSB under RCP4.5 and RCP8.5 scenarios would present noticeable differences in different seasons. In summer, 60–100% decreases are found for the south part of the basin, while in spring and winter, 60–100% increases are seen in the coastal part of the basin. The maximum change for the precipitation variable was obtained from the HadGEM model outputs, as in the temperature variable. According to the HadGEM

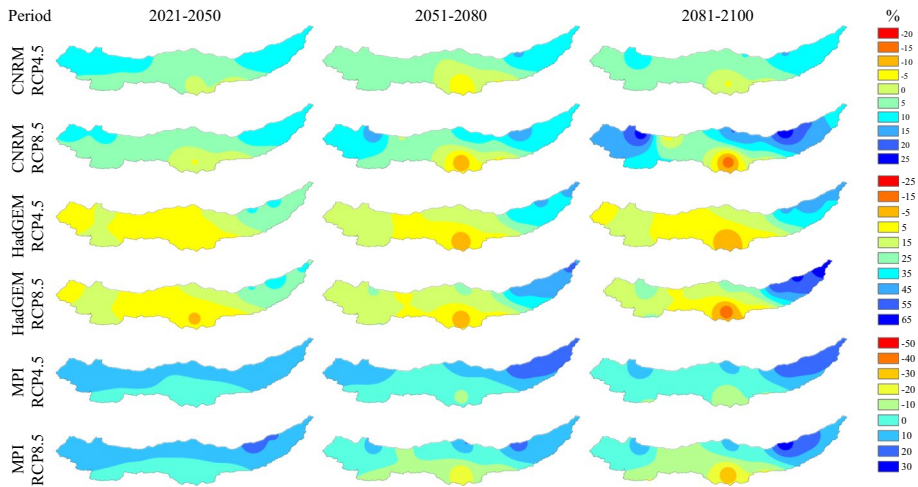


Fig. 10 Spatial distribution for the change of annual mean precipitation (compared to base period) in future periods under RCP4.5 and RCP8.5 scenarios

model results, the highest increase in precipitation occurs in the Pazar, Rize, and Hopa stations located on the coastline of the basin. Except for the Hopa, Pazar, and Rize stations, a decrease in precipitation is expected throughout the basin in the summer. The stations with the highest decrease are Bayburt, Giresun, and Şebinkarahisar.

The distributions of precipitation changes are shown in Fig. 10 for the considered future periods (2021–2050, 2051–2080, and 2081–2100) under two RCP scenarios. The annual total precipitation values decrease in the basin's interior. In addition, increases are generally on the coastline stations. The report by the Turkish State Meteorological Service evaluates the climate of Türkiye, attributing the situation to the country's irregular topography. Particularly, high mountains parallel to the Black Sea coast and located very close to the coastline prevent the passage of moist air and rain-laden clouds from the Black Sea into the inner regions. Rain clouds deposit much of their water content in the coastal areas (Sensoy et al. 2008). This situation is clearly evident from Table 2, which provides basic statistics based on observations. With climate change, increasing temperatures are expected to enhance the amount of evaporation from the surface of the Black Sea, leading to a greater amount of rainfall in coastal regions. Due to heavy precipitation, many flood events occurred in the sub-basins, where these stations are located. Therefore, foreseen precipitation increases in these stations may cause severe problems in the basin for future periods. At the same time, it is believed that decreases in precipitation may lead to drought problems for stations located south of the basin, which already has a dry climate. Therefore, this fact highlights the importance of swift adaptation and mitigation measures in the study areas (Al-Mukhtar and Qasim 2019). Similar findings, i.e., an increase in winter and spring precipitation, are projected in large-scale studies covering the basin (Bağçacı et al. 2021; Demircan et al. 2017; Turkes et al. 2020).

4.3 Intra-period and scenario trend results

Orographic precipitation prevails in the coastal areas because the mountains extend parallel to the sea in the EBSB (Fig. 2). At the same time, the continental climate is more dominant in the inland areas (Durukanoğlu 1996; Yüksek et al. 2013). Precipitation is also clustered differently in the interior and coastal regions of the basin and shows similar seasonality and cluster within themselves in the studies covering the basin (Akbas 2023; Kömüşçü et al. 2022; Türkeş et al. 2016; Zeybekoğlu and Keskin 2020). For these reasons, trend analyses were applied by calculating separate group averages of station data in interior and coastal regions. Then, when trend conditions for MK and ITST are analyzed at a 5% significance level, a greater than 5% change is determined for the percentage change in IVITA. The results of the analyses are given in Fig. 11 for monthly average temperature and Fig. 12 for monthly total precipitation.

According to MK, there is an increasing trend in both regions in months 8th and 11th, with an increasing trend in about all months and regions according to ITST for temperatures during the observation period (Fig. 11a, b). The increasing trend is clear in more than half of GCMs, scenarios, and periods for the future period according to both methods. However, there are more statistically significant months in ITST. Although there is general agreement in trends and directions among GCMs, there are some discrepancies, especially in months 1st, 2nd, and 12th. Regarding scenarios, RCP8.5 has a higher trend magnitude than RCP4.5 in inland regions, with no significant divergence in coastal regions. The trend magnitudes in the 2090s are also more pronounced in the interior compared to other

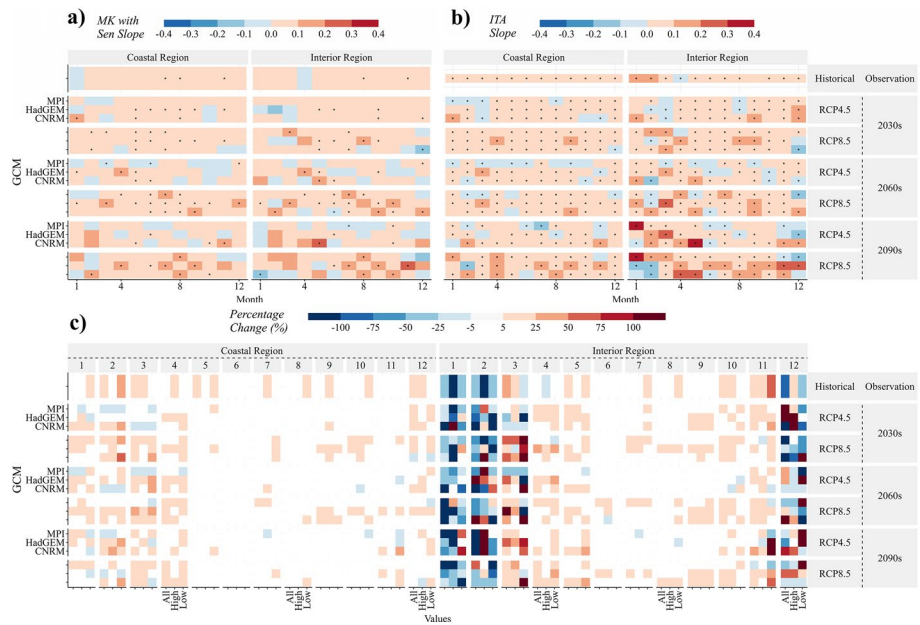


Fig. 11 Monotonic trends (a MK and b ITA) and high–low group trends (c IVITA) of the mean monthly temperature in the coastal and interior regions according to RCP4.5 and RCP8.5, and periods of observation, 2030s, 2060s, and 2090s

periods. In other words, this situation supports the temperature increases according to the observation in Fig. 8.

There is a general increasing trend in all, high and low values between the 12th–4th months in the coastal region (Fig. 11c). These periods also include the winter and spring. When the basic statistics of the basin are analyzed, it is seen that precipitation is especially high in the spring months. It is predicted that increases in precipitation during these periods may increase the risk of floods and landslides in the region. However, there are increasing and decreasing trends exceeding 100% in interior regions, except between the 4th–10th months. Besides, when the contribution of low and high values to all values is approximately similar in coastal regions, this situation changes in interior regions. The changes in the low and high values do not change at the same rate, and the 1st and 2nd months are the months with more than 25% difference between them and are more in the inland regions. During the observation period, in the coastal (interior) region, there is a trend in high values in the 4th, 7th, and 9th (4th) months, while there is no trend in all trends. That is, high values do not contribute. For future periods, the contribution of the low and high value trends to all trends together is seen in the interior region and between the 12th and 3rd months. Discrepancies in the direction of low and high value trends between these months are seen in different scenarios, GCMs, and periods. Regarding monotonic and group trends, MPI shows a more decreasing trend in the opposite direction than the other two GCMs.

It is seen in ITST that the monthly precipitation has monotonic trends in different directions in both regions during the observation period, while in MK, only in the coastal region, there is a significant decreasing trend in the 7th month and an increasing trend in the 8th–9th months (Fig. 12a, b). ITST results show significant decreasing trends generally dominate interior regions, while a slightly increasing trend dominates coastal regions.

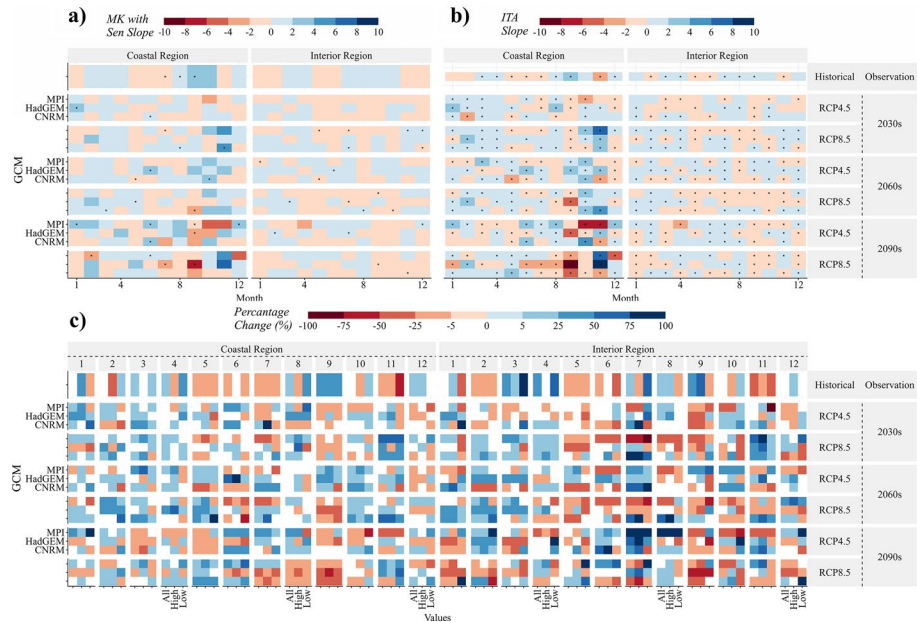


Fig. 12 Monotonic trends (a MK and b ITST) and all-high–low-group trends (c IVITA) of the mean monthly total precipitation in the coastal and interior regions according to RCP4.5 and RCP8.5, and periods of observation, 2030s, 2060s, and 2090s (*:5% significance level)

However, considering that even small increases in coastal areas carry risks for the region, it is possible to say that flood risks will increase. It is seen that there is no consistency between GCMs in trend existence and trend directions, especially in the coastal region. While there is a decreasing trend at month 11th in the observation period, there is an increasing trend in the RCP8.5 scenario in all GCMs in the 2030s in both regions.

There is a decreasing trend in the 5th, 7th, and 11th months in the coastal region and the 2nd, 5th, and 11th months in the interior region (Fig. 12c). There is an increasing trend in the 9th month in the coastal region and the 3rd month in the interior region in all data categories during the observation period. Changes in low and high values do not change at the same rate, and the months with more than 25% difference between them are generally the 1st and 7th months and are more frequent in interior regions. During the observation period, there is a trend in different directions in the low and high categories in months 1st, 2nd, 8th, and 10th (1st, 4th, 7th, and 8th) in the coastal (interior) region. While there is generally a trend in different directions in the low and high groups, there is no trend in all groups in the 1st, 10th, and 11th months. So, there is a need for caution against the behaviors of these months. In addition, about trend magnitude, the highest change is observed in the inner region in the 7th month. Although the trends of the groups may be in different directions in the future, there is usually a trend in the same direction. As in the ITST, there is a decreasing trend in the coastal region in the months 5th, 6th, and 11th, while there is a general increasing trend in all groups in the 2090s.

When the findings of the methods are analyzed, ITST shows a more significant trend than MK, while IVITA also shows more trends like ITST. However, IVITA shows a trend in the low and/or high groups, although it is not monotonic. Regarding the amount of change, trends exceed 100% in separate groups between 12th–3rd months in temperatures. Although temperatures mostly increase in intra-period averages according to observation averages (Figs. 7, 8), there are also decreases in monotonic and group trends during intra-periods (Fig. 11). Future temperature trends in groups are also more critical than precipitation. When the trend analyses are evaluated considering the coastal and inland areas of the basin, it is seen that the coastal and inland areas have different trend characteristics, which shows differences in the future period. When the basin characteristics are analyzed, it is seen that inland and coastal areas have quite different climatic characteristics. It can be stated that this situation is due to the basin's characteristics.

All the results obtained within this study's scope are obtained using the models' outputs in the CMIP5 archive. Although the most recent data set, CMIP6, has not been used, it is thought that it will provide a basis for local administrators, the people of the region, and researchers. It is thought that the findings obtained from this study prepared for the EBSB of Türkiye, which is frequently on the agenda with floods and landslides, causing many casualties and economic losses, will provide important data for future basin planning and water structures. The findings of this study are also considered important in terms of providing data for future downscaling studies and trend analysis studies using CMIP6 or different reanalysis data.

5 Conclusions

This study investigated the possible effects of climate change in the future on temperature and precipitation variables observed from 12 stations in the Eastern Black Sea Basin (EBSB), Türkiye. According to the main results obtained from the study, the MARS

statistical downscaling method can be applied as an alternative downscaling method to produce reasonable results in future studies to determine the effects of climate change. Based on the results of NS values, models applied for temperature and precipitation variables showed *very good* and *satisfactory/good* performance, respectively. Temperature increases were projected for the RCP4.5 and RCP8.5 scenarios throughout the basin. The highest temperature increases were seen in the summer months for all stations. In the summer months, increases of up to 10 °C are predicted for all GCM and scenarios at Gümüşhane, Bayburt, Şebinkarahisar, and Susehri stations, which are located in the interior region and have continental climate characteristics. Although the results for all three GCM models were similar, the highest and lowest temperature increase models were HadGEM2-ES and MPI-ESM-MR, respectively.

When the simulated precipitation values for the future period are compared with the base period, the monthly and annual total precipitation values show different patterns of variation for three different periods throughout the basin under the RCP4.5 and RCP8.5 scenarios. The precipitation of the stations in the interior part of the basin was observed to decrease by 100% in the summer months, and there would be a 50% increase in the spring months. A drier future is expected in the south due to the increasing temperature and decreasing precipitation in the summer months. In addition, it is observed that precipitation in Rize, Pazar, and Hopa stations located in the eastern part of the basin will increase by 100% in spring. The floods in this region in the past years, especially in the spring, may increase due to short-term heavy precipitation and melting snow with increasing temperatures. It is also predicted that the climate of the EBSB, known to be wet in all seasons, will change with the decrease in precipitation for the summer and autumn seasons.

Furthermore, although a general increase in temperature averages is more pronounced than in precipitation averages, the different trends of low and high groups within periods contribute to all data trends. The percentages of temperature change in the low and high groups and all data are more pronounced for precipitation. However, GCMs generally show different monotonic and group trends in different directions in inland regions compared to coastal regions, which may indicate that uncertainty may be higher in continental climates. It is also concluded that the interior and coastal regions of the basin will maintain their differences in the future. In conclusion, the difference in trend direction between different groups and GCMs in interior regions may indicate that there may be more uncertainty than in coastal regions.

This study has shown that climate change under certain future scenarios may seriously affect the hydrology and water resources of the EBSB. Knowing the possible effects of climate change on temperature and precipitation, the essential hydrological variables can provide basic information for ecological, economic, social, and health decision-makers. The authors suggest further assessing the study area with different statistical downscaling methods using a large ensemble of CMIP5 and CMIP6 data sets forced under different emission and social scenarios. In addition, the contribution of downscaling models developed using different reanalysis data to model performance can be examined. Daily, monthly, seasonal, and annual changes and cycles of other climatic variables such as maximum temperature, minimum temperature, wet period length, and dry period length can be investigated with more comparative performance statistics.

Acknowledgements The authors are grateful to the providers of the Salford Predictive Modeler 8 software employed to perform the MARS analysis. Also, the authors would like to thank the anonymous reviewers for their constructive comments and suggestions, which helped improve the paper. The authors sincerely thank the personnel of Turkish State Meteorological Service for data monitoring, processing, and management.

Author contributions Conceptualization, S.N. and M.K.; Investigation, S.N. and M.S.; Methodology, S.N., M.S., M.K., and U.O.; Supervision, M.K., and U.O.; Visualization, S.N. and M.S.; Writing-original draft preparation, S.N.; Writing, review, and editing, S.N., M.K., U.O., and M.S.

Funding Open access funding provided by the Scientific and Technological Research Council of Türkiye (TÜBİTAK). This research received no external funding.

Data availability Some or all data that support this study finding are available from the corresponding author upon reasonable request.

Code availability The models or codes used to develop this study are available from the corresponding author upon reasonable request.

Declarations

Conflict of interest The authors declare that they have no conflict of interest.

Ethical approval Not applicable.

Consent to Participate Not applicable.

Consent to Publish Not applicable.

Open Access This article is licensed under a Creative Commons Attribution 4.0 International License, which permits use, sharing, adaptation, distribution and reproduction in any medium or format, as long as you give appropriate credit to the original author(s) and the source, provide a link to the Creative Commons licence, and indicate if changes were made. The images or other third party material in this article are included in the article's Creative Commons licence, unless indicated otherwise in a credit line to the material. If material is not included in the article's Creative Commons licence and your intended use is not permitted by statutory regulation or exceeds the permitted use, you will need to obtain permission directly from the copyright holder. To view a copy of this licence, visit <http://creativecommons.org/licenses/by/4.0/>.

References

- Abbasnia M, Tavousi T, Khosravi M (2016) Assessment of future changes in the maximum temperature at selected stations in Iran based on HADCM3 and CGCM3 models. *Asia-Pac J Atmos Sci* 52(4):371–377. <https://doi.org/10.1007/s13143-016-0006-z>
- Achite M, Simsek O, Adarsh S, Hartani T, Caloiero T (2023) Assessment and monitoring of meteorological and hydrological drought in semiarid regions: the Wadi Ouahrane basin case study (Algeria). *Phys Chem Earth Parts A/B/C* 130:103386. <https://doi.org/10.1016/j.pce.2023.103386>
- Akbas A (2023) Seasonality, persistency, regionalization, and control mechanism of extreme rainfall over complex terrain. *Theoret Appl Climatol* 152(3–4):981–997. <https://doi.org/10.1007/s00704-023-04440-1>
- Akçay F, Kankal M, Şan M (2022) Innovative approaches to the trend assessment of streamflows in the Eastern Black Sea basin, Turkey. *Hydrol Sci J* 67(2):222–247. <https://doi.org/10.1080/02626667.2021.1998509>
- Aliyazıcıoğlu Ş, Öztürk KF, Günen MA (2023) Analysis of Gümüşhane-Trabzon highway slope static and dynamic behavior using point cloud data. *Adv Lidar* 3(2):70–75
- Al-Mukhtar M, Qasim M (2019) Future predictions of precipitation and temperature in Iraq using the statistical downscaling model. *Arab J Geosci* 12(2):25. <https://doi.org/10.1007/s12517-018-4187-x>
- Amjad M, Yilmaz MT, Yucel I, Yilmaz KK (2020) Performance evaluation of satellite- and model-based precipitation products over varying climate and complex topography. *J Hydrol* 584:124707. <https://doi.org/10.1016/j.jhydrol.2020.124707>
- Anılan T, Satılmış U, Kankal M, Yüksek O (2016) Application of artificial neural networks and regression analysis to L-moments based regional frequency analysis in the Eastern Black Sea Basin, Turkey. *KSCSE J Civil Eng* 20(5):2082–2092. <https://doi.org/10.1007/s12205-015-0143-4>

- Araya-Osses D, Casanueva A, Román-Figueroa C, Uribe JM, Paneque M (2020) Climate change projections of temperature and precipitation in Chile based on statistical downscaling. *Clim Dyn* 54(9–10):4309–4330. <https://doi.org/10.1007/s00382-020-05231-4>
- Arnell NW, Gosling SN (2016) The impacts of climate change on river flood risk at the global scale. *Clim Change* 134(3):387–401. <https://doi.org/10.1007/s10584-014-1084-5>
- Bağçacı SÇ, Yücel I, Düzenli E, Yılmaz MT (2021) Intercomparison of the expected change in the temperature and the precipitation retrieved from CMIP6 and CMIP5 climate projections: a Mediterranean hot spot case, Turkey. *Atmos Res* 256:105576. <https://doi.org/10.1016/j.atmosres.2021.105576>
- Bayazit M, Avci I (1997) Water resources of Turkey: potential, planning, development and management. *Int J Water Resour Dev* 13(4):443–452. <https://doi.org/10.1080/07900629749566>
- Bayer Altın T, Altın BN (2021) Response of hydrological drought to meteorological drought in the eastern Mediterranean Basin of Turkey. *J Arid Land* 13(5):470–486. <https://doi.org/10.1007/s40333-021-0064-7>
- Bilgili M, Bilirgen H, Ozbek A, Ekinci F, Demirdelen T (2018) The role of hydropower installations for sustainable energy development in Turkey and the world. *Renew Energy* 126:755–764. <https://doi.org/10.1016/j.renene.2018.03.089>
- Campozano L, Tenelanda D, Sanchez E, Samaniego E, Feyen J (2016) Comparison of statistical downscaling methods for monthly total precipitation: case study for the Paute River Basin in Southern Ecuador. *Adv Meteorol* 6526341. <https://doi.org/10.1155/2016/6526341>
- Cannon AJ, Sobie SR, Murdock TQ (2015) Bias correction of GCM precipitation by quantile mapping: how well do methods preserve changes in quantiles and extremes? *J Clim* 28(17):6938–6959. <https://doi.org/10.1175/JCLI-D-14-00754.1>
- Chen J, Brissette FP, Leconte R (2011) Uncertainty of downscaling method in quantifying the impact of climate change on hydrology. *J Hydrol* 401(3–4):190–202. <https://doi.org/10.1016/j.jhydrol.2011.02.020>
- Crane RG, Hewitson BC (1998) Doubled CO₂ precipitation changes for the Susquehanna Basin: downscaling from the Genesis general circulation model. *Int J Climatol* 18(1):65–76. [https://doi.org/10.1002/\(SICI\)1097-0088\(199801\)18:1%3c65::AID-JOC222%3e3.0.CO;2-9](https://doi.org/10.1002/(SICI)1097-0088(199801)18:1%3c65::AID-JOC222%3e3.0.CO;2-9)
- Dabanlı İ, Şen Z, Yeleğen MÖ, Şişman E, Seleğ B, Güçlü YS (2016) Trend assessment by the innovative-Şen method. *Water Resour Manage* 30(14):5193–5203. <https://doi.org/10.1007/s11269-016-1478-4>
- Demircan M, Gürkan H, Eskioglu O, Arabacı H, Coşkun M (2017) Climate change projections for Turkey: three models and two scenarios. *Turk J Water Sci Manag* 1(1):22–43. <https://doi.org/10.31807/tjwsm.297183>
- Dey P, Das AK (2016) Application of multivariate adaptive regression spline-assisted objective function on optimization of heat transfer rate around a cylinder. *Nucl Eng Technol* 48(6):1315–1320. <https://doi.org/10.1016/j.net.2016.06.011>
- Dibike YB, Gachon P, St-Hilaire A, Ouarda TBMJ, Nguyen VTV (2008) Uncertainty analysis of statistically downscaled temperature and precipitation regimes in Northern Canada. *Theoret Appl Climatol* 91(1–4):149–170. <https://doi.org/10.1007/s00704-007-0299-z>
- Durukanoglu HF (1996) Orographic precipitation in the Southern Black Sea Coasts. In: *Climate sensitivity to radiative perturbations*. Springer, Berlin, pp 317–324. https://doi.org/10.1007/978-3-642-61053-0_24
- Fiebig-Wittmaack M, Astudillo O, Wheaton E, Wittrock V, Perez C, Ibacache A (2012) Climatic trends and impact of climate change on agriculture in an arid Andean valley. *Clim Change* 111(3):819–833. <https://doi.org/10.1007/s10584-011-0200-z>
- Fistikoglu O, Okkan U (2011) Statistical downscaling of monthly precipitation using NCEP/NCAR reanalysis data for Tahtali River Basin in Turkey. *J Hydrol Eng* 16(2):157–164. [https://doi.org/10.1061/\(ASCE\)HE.1943-5584.0000300](https://doi.org/10.1061/(ASCE)HE.1943-5584.0000300)
- Friedman JH, Roosen CB (1995) An introduction to multivariate adaptive regression splines. *Stat Methods Med Res* 4(3):197–217. <https://doi.org/10.1177/096228029500400303>
- Friedman JH (1991) Multivariate adaptive regression splines. *Ann Stat* 19(1):1–67. <http://www.jstor.org/stable/2241837>
- Gebre SL, Ludwig F (2015) Hydrological response to climate change of the upper Blue Nile River Basin: based on IPCC fifth assessment report (AR5). *J Climatol Weather Forecast* 3(1):1–15. <https://doi.org/10.4172/2332-2594.1000121>
- Ghiaei F, Kankal M, Anilan T, Yuksek O (2018) Regional intensity–duration–frequency analysis in the Eastern Black Sea Basin, Turkey, by using L-moments and regression analysis. *Theoret Appl Climatol* 131(1–2):245–257. <https://doi.org/10.1007/s00704-016-1953-0>
- Görüm T, Fidan S (2021) Spatiotemporal variations of fatal landslides in Turkey. *Landslides* 18(5):1691–1705. <https://doi.org/10.1007/s10346-020-01580-7>

- Güçlü YS (2020) Improved visualization for trend analysis by comparing with classical Mann–Kendall test and ITA. *J Hydrol* 584:124674. <https://doi.org/10.1016/j.jhydrol.2020.124674>
- Günen MA, Atasever UH (2024) Remote sensing and monitoring of water resources: a comparative study of different indices and thresholding methods. *Sci Total Environ* 926:172117. <https://doi.org/10.1016/j.scitotenv.2024.172117>
- Guo Q, Chen J, Zhang X, Shen M, Chen H, Guo S (2019) A new two-stage multivariate quantile mapping method for bias correcting climate model outputs. *Clim Dyn* 53(5–6):3603–3623. <https://doi.org/10.1007/s00382-019-04729-w>
- Güven A, Pala A, Sheikhsaisi M (2021) Investigation of impact of climate change on small catchments using different climate models and statistical approaches. *Water Supply* 22(3):3540–3552. <https://doi.org/10.2166/ws.2021.383>
- Haltas I, Yildirim E, Oztas F, Demir I (2021) A comprehensive flood event specification and inventory: 1930–2020 Turkey case study. *Int J Disaster Risk Red* 56:102086. <https://doi.org/10.1016/j.ijdrr.2021.102086>
- Hamed KH, Rao AR (1998) A modified Mann-Kendall trend test for autocorrelated data. *J Hydrol* 204(1–4):182–196. [https://doi.org/10.1016/S0022-1694\(97\)00125-X](https://doi.org/10.1016/S0022-1694(97)00125-X)
- Hassan Z, Shamsudin S, Harun S (2014) Application of SDSM and LARS-WG for simulating and downscaling of rainfall and temperature. *Theoret Appl Climatol* 116(1–2):243–257. <https://doi.org/10.1007/s00704-013-0951-8>
- Huang J, Zhang J, Zhang Z, Xu C, Wang B, Yao J (2011) Estimation of future precipitation change in the Yangtze River basin by using statistical downscaling method. *Stoch Env Res Risk Assess* 25(6):781–792. <https://doi.org/10.1007/s00477-010-0441-9>
- Huang H, Ji X, Xia F, Huang S, Shang X, Chen H, Zhang M, Dahlgren RA, Mei K (2020) Multivariate adaptive regression splines for estimating riverine constituent concentrations. *Hydrol Process* 34(5):1213–1227. <https://doi.org/10.1002/hyp.13669>
- Huntingford C, Lowe JA, Howarth N, Bowerman NH, Gohar LK, Otto A et al (2015) The implications of carbon dioxide and methane exchange for the heavy mitigation RCP2.6 scenario under two metrics. *Environ Sci Policy* 51:77–87. <https://doi.org/10.1016/j.envsci.2015.03.013>
- Kang B, Moon S (2017) Regional hydroclimatic projection using an coupled composite downscaling model with statistical bias corrector. *KSCE J Civ Eng* 21(7):2991–3002. <https://doi.org/10.1007/s12205-017-1176-7>
- Kaygusuz K (2018) Small hydropower potential and utilization in Turkey. *J Eng Res Appl Sci* 7(1):791–798. <http://journaleras.com/index.php/jeras/article/view/110>
- Khuntia S, Mujtaba H, Patra C, Farooq K, Sivakugan N, Das BM (2015) Prediction of compaction parameters of coarse grained soil using multivariate adaptive regression splines (MARS). *Int J Geotech Eng* 9(1):79–88. <https://doi.org/10.1179/1939787914Y.0000000061>
- Kim S, Joo K, Kim H, Shin JY, Heo JH (2020) Regional quantile delta mapping method using regional frequency analysis for regional climate model precipitation. *J Hydrol* 596:125685. <https://doi.org/10.1016/j.jhydrol.2020.125685>
- Knutti R, Furrer R, Tebaldi C, Cernak J, Meehl GA (2010) Challenges in combining projections from multiple climate models. *J Clim* 23(10):2739–2758. <https://doi.org/10.1175/2009JCLI3361.1>
- Kömüçü AÜ, Turgu E, DeLiberty T (2022) Dynamics of precipitation regions of Turkey: a clustering approach by K-means methodology in respect of climate variability. *J Water Clim Change* 13(10):3578–3606. <https://doi.org/10.2166/wcc.2022.186>
- Körük AE, Kankal M, Yıldız MB, Akçay F, Şan M, Nacar S (2023) Trend analysis of precipitation using innovative approaches in northwestern Turkey. *Phys Chem Earth Parts A/B/C* 131:103416. <https://doi.org/10.1016/j.pce.2023.103416>
- Kumar S, Merwade V, Kam J, Thurner K (2009) Streamflow trends in Indiana: effects of long term persistence, precipitation and subsurface drains. *J Hydrol* 374(1–2):171–183. <https://doi.org/10.1016/j.jhydrol.2009.06.012>
- Liu Z, Liu Y, Wang S, Yang X, Wang L, Baig MHA, Chi W, Wang Z (2018) Evaluation of spatial and temporal performances of ERA-interim precipitation and temperature in Mainland China. *J Clim* 31(11):4347–4365. <https://doi.org/10.1175/JCLI-D-17-0212.1>
- Mekonnen FD, Disse M (2018) Analyzing the future climate change of Upper Blue Nile River basin using statistical downscaling techniques. *Hydrol Earth Syst Sci* 22(4):2391–2408. <https://doi.org/10.5194/hess-22-2391-2018>
- Moriasi DN, Arnold JG, Van Liew MW, Bingner RL, Harmel RD, Veith TL (2007) Model evaluation guidelines for systematic quantification of accuracy in watershed simulations. *Trans ASABE* 50(3):885–900. <https://doi.org/10.13031/2013.23153>

- Nacar S, Bayram A, Baki OT, Kankal M, Aras E (2020) Spatial forecasting of dissolved oxygen concentration in the Eastern Black Sea Basin. *Turkey Water* 12(4):1041. <https://doi.org/10.3390/w12041041>
- Nourani V, Razzaghzadeh Z, Baghanam AH, Molajou A (2019) ANN-based statistical downscaling of climatic parameters using decision tree predictor screening method. *Theoret Appl Climatol* 137(3–4):1729–1746. <https://doi.org/10.1007/s00704-018-2686-z>
- Nuri Balov M, Altunkaynak A (2020) Spatio-temporal evaluation of various global circulation models in terms of projection of different meteorological drought indices. *Environ Earth Sci* 79(6):126. <https://doi.org/10.1007/s12665-020-8881-0>
- Okkan U, Fistikoglu O (2014) Evaluating climate change effects on runoff by statistical downscaling and hydrological model GR2M. *Theoret Appl Climatol* 117(1):343–361. <https://doi.org/10.1007/s00704-013-1005-y>
- Okkan U, Inan G (2015a) Bayesian learning and relevance vector machines approach for downscaling of monthly precipitation. *J Hydrol Eng* 20(4):04014051. [https://doi.org/10.1061/\(asce\)jhe.1943-5584.0001024](https://doi.org/10.1061/(asce)jhe.1943-5584.0001024)
- Okkan U, Inan G (2015b) Statistical downscaling of monthly reservoir inflows for Kemer watershed in Turkey: use of machine learning methods, multiple GCMs and emission scenarios. *Int J Climatol* 35(11):3274–3295. <https://doi.org/10.1002/joc.4206>
- Okkan U, Kirdemir U (2016) Downscaling of monthly precipitation using CMIP5 climate models operated under RCPs. *Meteorol Appl* 23(3):514–528. <https://doi.org/10.1002/met.1575>
- Okkan U, Kirdemir U (2018) Investigation of the behavior of an agricultural-operated dam reservoir under RCP scenarios of AR5-IPCC. *Water Resour Manage* 32(8):2847–2866. <https://doi.org/10.1007/s11269-018-1962-0>
- Okkan U, Fistikoglu O, Ersoy ZB, Noori AT (2023) Investigating adaptive hedging policies for reservoir operation under climate change impacts. *J Hydrol* 619:129286. <https://doi.org/10.1016/j.jhydrol.2023.129286>
- Okkan U, Fistikoglu O, Ersoy ZB, Noori AT (2024) Analyzing the uncertainty of potential evapotranspiration models in drought projections derived for a semi-arid watershed. *Theor Appl Climatol* 155(3):2329–2346. <https://doi.org/10.1007/s00704-023-04817-2>
- Önöz B, Bayazit M (2003) The power of statistical tests for trend detection. *Turk J Eng Environ Sci* 27(4):247–251
- Ouhamdouch S, Bahir M (2017) Climate change impact on future rainfall and temperature in semi-arid areas (Essaouira Basin, Morocco). *Environ Process* 4(4):975–990. <https://doi.org/10.1007/s40710-017-0265-4>
- Pan JF, van den Dool H (1998) Extended-range probability forecasts based on dynamical model output. *Weather Forecast* 13(4):983–996. [https://doi.org/10.1175/1520-0434\(1998\)013%3c0983:ERPFB0%3e2.0.CO;2](https://doi.org/10.1175/1520-0434(1998)013%3c0983:ERPFB0%3e2.0.CO;2)
- Pechlivanidis IG, Arheimer B, Donnelly C, Hundecha Y, Huang S, Aich V, Samaniego L, Eisner S, Shi P (2017) Analysis of hydrological extremes at different hydro-climatic regimes under present and future conditions. *Clim Change* 141(3):467–481. <https://doi.org/10.1007/s10584-016-1723-0>
- Pettitt AN (1979) A non-parametric approach to the change-point problem. *Appl Stat* 28(2):126. <https://doi.org/10.2307/2346729>
- Reiter P, Gutjahr O, Schefczyk L, Heinemann G, Casper M (2018) Does applying quantile mapping to subsamples improve the bias correction of daily precipitation? *Int J Climatol* 38(4):1623–1633. <https://doi.org/10.1002/joc.5283>
- Riahi K, Rao S, Krey V, Cho C, Chirkov V, Fischer G, Kindermann G, Nakicenovic N, Rafaj P (2011) RCP 8.5-A scenario of comparatively high greenhouse gas emissions. *Clim Change* 109(1):33–57. <https://doi.org/10.1007/s10584-011-0149-y>
- Sachindra DA, Huang F, Barton A, Perera BJC (2014) Statistical downscaling of general circulation model outputs to precipitation-part 2: Bias-correction and future projections. *Int J Climatol* 34(11):3282–3303. <https://doi.org/10.1002/joc.3915>
- Salmani-Dehaghi N, Samani N (2021) Development of bias-correction PERSIANN-CDR models for the simulation and completion of precipitation time series. *Atmos Environ* 246:117981. <https://doi.org/10.1016/j.atmosenv.2020.117981>
- Samui P (2013) Multivariate adaptive regression spline (Mars) for prediction of elastic modulus of jointed rock mass. *Geotech Geol Eng* 31(1):249–253. <https://doi.org/10.1007/s10706-012-9584-4>
- Şan M, Akçay F, Linh NTT, Kankal M, Pham QB (2021) Innovative and polygonal trend analysis applications for rainfall data in Vietnam. *Theoret Appl Climatol* 144(3–4):809–822. <https://doi.org/10.1007/s00704-021-03574-4>

- Şan M, Nacar S, Kankal M, Bayram A (2023) Daily precipitation performances of regression-based statistical downscaling models in a basin with mountain and semi-arid climates. *Stoch Env Res Risk Assess* 37(4):1431–1455. <https://doi.org/10.1007/s00477-022-02345-5>
- Schroerer K, Kirchengast G (2018) Sensitivity of extreme precipitation to temperature: the variability of scaling factors from a regional to local perspective. *Clim Dyn* 50(11–12):3981–3994. <https://doi.org/10.1007/s00382-017-3857-9>
- Semadeni-Davies A, Hernebring C, Svensson G, Gustafsson LG (2008) The impacts of climate change and urbanisation on drainage in Helsingborg, Sweden: combined sewer system. *J Hydrol* 350(1–2):100–113. <https://doi.org/10.1016/j.jhydrol.2007.05.028>
- Şen Z (2012) Innovative trend analysis methodology. *J Hydrol Eng* 17(9):1042–1046. [https://doi.org/10.1061/\(ASCE\)HE.1943-5584.0000556](https://doi.org/10.1061/(ASCE)HE.1943-5584.0000556)
- Şen Z (2017) Innovative trend significance test and applications. *Theoret Appl Climatol* 127(3–4):939–947. <https://doi.org/10.1007/s00704-015-1681-x>
- Sensoy S, Demircan M, Ulupinar Y, Balta I (2008) Climate of Turkey. *Turk State Meteorol Serv* 401:1–13
- Serbes ZA, Yildirim T, Mengu GP, Akkuzu E, Asik S, Okkan U (2019) Temperature and precipitation projections under AR4 scenarios: the case of Kucuk Menderes basin, Turkey. *J Environ Prot Ecol* 20(1):44–51
- Singh J, Knapp HV, Arnold JG, Demissie M (2005) Hydrological modeling of the Iroquois River watershed using HSPF and SWAT. *J Am Water Resour Assoc* 41(2):343–360. <https://doi.org/10.1111/j.1752-1688.2005.tb03740.x>
- Sonali P, Kumar DN (2013) Review of trend detection methods and their application to detect temperature changes in India. *J Hydrol* 476:212–227. <https://doi.org/10.1016/j.jhydrol.2012.10.034>
- Souvignt M, Gaesse H, Ribbe L, Kretschmer N, Oyarzún R (2010) Statistical downscaling of precipitation and temperature in north-central Chile: an assessment of possible climate change impacts in an arid Andean watershed. *Hydrol Sci J* 55(1):41–57. <https://doi.org/10.1080/02626660903526045>
- Suman S, Khan SZ, Das SK, Chand SK (2016) Slope stability analysis using artificial intelligence techniques. *Nat Hazards* 84(2):727–748. <https://doi.org/10.1007/s11069-016-2454-2>
- Taylor KE, Stouffer RJ, Meehl GA (2012) An overview of CMIP5 and the experiment design. *Bull Am Meteor Soc* 93(4):485–498. <https://doi.org/10.1175/BAMS-D-11-00094.1>
- Thomson AM, Calvin KV, Smith SJ, Kyle GP, Volke A, Patel P, Delgado-Arias S, Bond-Lamberty B, Wise MA, Clarke LE, Edmonds JA (2011) RCP4.5: a pathway for stabilization of radiative forcing by 2100. *Clim Change* 109(1):77–94. <https://doi.org/10.1007/s10584-011-0151-4>
- Tiryaki S, Tan H, Bardak S, Kankal M, Nacar S, Peker H (2019) Performance evaluation of multiple adaptive regression splines, teaching–learning based optimization and conventional regression techniques in predicting mechanical properties of impregnated wood. *Eur J Wood Wood Products* 77(4):645–659. <https://doi.org/10.1007/s00107-019-01416-9>
- Tongal H (2019) Spatiotemporal analysis of precipitation and extreme indices in the Antalya Basin, Turkey. *Theor Appl Climatol* 138(3–4):1735–1754. <https://doi.org/10.1007/s00704-019-02927-4>
- Tripathi S, Srinivas VV, Nanjundiah RS (2006) Downscaling of precipitation for climate change scenarios: a support vector machine approach. *J Hydrol* 330(3–4):621–640. <https://doi.org/10.1016/j.jhydrol.2006.04.030>
- Türkeş M, Yozgatlıgil C, Batmaz İ, Yiğün C, Kartal Koç E, Fahmi F, Aslan S (2016) Has the climate been changing in Turkey? Regional climate change signals based on a comparative statistical analysis of two consecutive time periods, 1950–1980 and 1981–2010. *Climate Res* 70(1):77–93. <https://doi.org/10.3354/cr01410>
- Turkes M, Turp MT, An N, Ozturk T, Kurnaz ML (2020) Impacts of climate change on precipitation climatology and variability in Turkey. In: Harmancioglu NB, Altinbilek D (eds) *Water resources of Turkey*, pp 467–491. https://doi.org/10.1007/978-3-030-11729-0_14
- Wayne GP (2013) Representative concentration pathways (RCPs). *Sceptical Sci* 1:1–24
- Wilby RL, Wigley TML (1997) Downscaling general circulation model output: a review of methods and limitations. *Progr Phys Geogr Earth Environ* 21(4):530–548. <https://doi.org/10.1177/030913339702100403>
- Wilby RL, Hassan H, Hanaki K (1998) Statistical downscaling of hydrometeorological variables using general circulation model output. *J Hydrol* 205(1–2):1–19. [https://doi.org/10.1016/S0022-1694\(97\)00130-3](https://doi.org/10.1016/S0022-1694(97)00130-3)
- Wilby RL, Dawson CW, Barrow EM (2002) SDSM—a decision support tool for the assessment of regional climate change impacts. *Environ Model Softw* 17(2):145–157. [https://doi.org/10.1016/s1364-8152\(01\)00060-3](https://doi.org/10.1016/s1364-8152(01)00060-3)

- Wilby RL, Charles SP, Zorita E, Timbal B, Whetton P, Mearns LO (2004) Guidelines for use of climate scenarios developed from statistical downscaling methods. http://www.ctn.etsmtl.ca/cours/mgc921/dgm_no2_v1_09_2004.pdf
- Yang T, Li H, Wang W, Xu CY, Yu Z (2012) Statistical downscaling of extreme daily precipitation, evaporation, and temperature and construction of future scenarios. *Hydrol Process* 26(23):3510–3523. <https://doi.org/10.1002/hyp.8427>
- Yao N, Li L, Feng P, Feng H, Liu DL, Liu Y, Jiang K, Hu X, Li Y (2020) Projections of drought characteristics in China based on a standardized precipitation and evapotranspiration index and multiple GCMs. *Sci Total Environ* 704:135245. <https://doi.org/10.1016/j.scitotenv.2019.135245>
- Yüksek Ö, Kankal M, Üçüncü O (2013) Assessment of big floods in the Eastern Black Sea Basin of Turkey. *Environ Monit Assess* 185(1):797–814. <https://doi.org/10.1007/s10661-012-2592-2>
- Zeybekoğlu U, Keskin AÜ (2020) Defining rainfall intensity clusters in Turkey by using the fuzzy c-means algorithm. *Geofizika* 37(2):181–195. <https://doi.org/10.15233/gfz.2020.37.8>
- Zhang W, Goh ATC (2016) Multivariate adaptive regression splines and neural network models for prediction of pile drivability. *Geosci Front* 7(1):45–52. <https://doi.org/10.1016/j.gsf.2014.10.003>
- Zhang Q, Xu C-Y, Tao H, Jiang T, Chen YD (2010) Climate changes and their impacts on water resources in the arid regions: a case study of the Tarim River basin, China. *Stoch Env Res Risk Assess* 24(3):349–358. <https://doi.org/10.1007/s00477-009-0324-0>
- Zhang W, Wu C, Li Y, Wang L, Samui P (2021) Assessment of pile drivability using random forest regression and multivariate adaptive regression splines. *Georisk Assess Manag Risk Eng Syst Geohaz* 15(1):27–40. <https://doi.org/10.1080/17499518.2019.1674340>
- Zhao T, Bennett JC, Wang QJ, Schepen A, Wood AW, Robertson DE, Ramos MH (2017) How suitable is quantile mapping for postprocessing GCM precipitation forecasts? *J Clim* 30(9):3185–3196. <https://doi.org/10.1175/JCLI-D-16-0652.1>

Publisher's Note Springer Nature remains neutral with regard to jurisdictional claims in published maps and institutional affiliations.

Authors and Affiliations

Sinan Nacar¹  · Murat Şan²  · Murat Kankal³  · Umut Okkan⁴ 

✉ Sinan Nacar
sinan.nacar@gop.edu.tr; sinannacar@hotmail.com

Murat Şan
muratsan@gumushane.edu.tr; stmuratsan@protonmail.com

Murat Kankal
mkankal@uludag.edu.tr

Umut Okkan
umutokkan@balikesir.edu.tr

¹ Department of Civil Engineering, Tokat Gaziosmanpaşa University, 60150 Tokat, Türkiye

² Department of Civil Engineering, Gümüşhane University, 29100 Gümüşhane, Türkiye

³ Department of Civil Engineering, Bursa Uludağ University, 16059 Bursa, Türkiye

⁴ Department of Civil Engineering, Balıkesir University, 10600 Balıkesir, Türkiye